

1 **Fault-controlled dolomitization in the Montagna dei Fiori Anticline (Central Apennines,**  
2 **Italy): Record of a dominantly pre-orogenic fluid migration**

3 Mahtab Mozafari<sup>1</sup>, Rudy Swennen<sup>2</sup>, Fabrizio Balsamo<sup>1</sup>, Hamdy El Desouky<sup>2,3</sup>, Fabrizio Storti<sup>1</sup>  
4 and Conxita Taberner<sup>4</sup>

5  
6 *1- NEXT - Natural and Experimental Tectonics Research Group - Department of Chemistry,*  
7 *Life Sciences and Environmental Sustainability, University of Parma, Italy.*

8 *2- Department of Earth and Environmental Sciences, KU Leuven, Belgium.*

9 *3- Geology Department, Faculty of Science, Menoufia University, Menoufia, Egypt*

10 *4- Shell Global Solutions International B.V., Amsterdam, The Netherlands*

11 Correspondence: Mahtab Mozafari (mahtab\_mozafari@yahoo.com) and Fabrizio Storti  
12 (Fabrizio.Storti@unipr.it)

13

14 **Abstract**

15 The Lower Jurassic platform and basinal deposits exposed in the Montagna dei Fiori  
16 Anticline (Central Apennines, Italy) are pervasively affected by dolomitization. Based on the  
17 integration of field work, petrography, and geochemistry, two fault-related dolomitization events  
18 were recognized and interpreted as occurred before and during the Apenninic orogeny,  
19 respectively. Fluid inclusion analysis indicates moderate to elevated salinity values of 3.5 to 20.5  
20 and 12.8 to 18.6 eq. wt. % NaCl, in the first and the second event, respectively. The estimated  
21 salinities, in combination with  $\delta^{18}\text{O}$  values and  $^{87}\text{Sr}/^{86}\text{Sr}$  ratios, suggest significant involvement  
22 of evaporitic fluids in both events, most likely derived from the underlying Upper Triassic  
23 Burano Formation. In addition, the  $^{87}\text{Sr}/^{86}\text{Sr}$  ratios up to 0.70963 suggest the circulation of deep-  
24 sourced fluids that interacted with siliciclastics and/or the crystalline basement during the  
25 dolomitization events. ~~The first dolomitization event which is also considered as the most~~  
26 ~~pervasive one started prior to the significant burial conditions, as reflected in homogenization~~  
27 ~~temperatures of their fluid inclusions being mostly below about 40-50°C.~~ Two major dolomite  
28 types (D1 and D2) were recognized as pertaining to ~~this the first~~ event, both postdated by high  
29 amplitude bed-parallel stylolites. ~~, supporting This relationship supports~~ a syn-burial, pre layer-  
30 parallel shortening dolomitization, ~~interpreted as controlled by the extensional fault pattern~~  
31 ~~affecting the carbonate succession before its involvement in the Apenninic thrust wedge.~~ A

32 possible geodynamic framework for this dolomitization event is Early to Late Jurassic rift-related  
33 extensional tectonism. ~~The second dolomitization event (D3, D4 and D5) initiated with a~~  
34 ~~dolomite type (D3) is~~ characterized by a slight temperature upturn (up to 73°C), followed by a  
35 ~~second type (D4) with markedly higher homogenization temperatures~~ (up to 105°C), and  
36 interpreted as associated with the inflow of hydrothermal fluids, possibly related to major  
37 changes in the permeability architecture of faults during early- to syn-thrusting and folding  
38 activity. ~~Eventually, D4 was overprinted by a late generation of dolomite veins (D5) interpreted~~  
39 ~~as associated with late orogenic extensional faulting in the backlimb of the Montagna dei Fiori~~  
40 ~~Anticline.~~ Based on the timing of deformation in the Montagna dei Fiori Anticline, ~~D3 to D5~~ the  
41 second dolomitization event likely occurred in Late Miocene to Pliocene times. The findings  
42 regarding characteristics and timing of dolomitization here illustrates the long-term controlling  
43 role of the evaporitic detachments in dolomitization process. Our data shows the Mg-rich fluids  
44 most likely derived from these evaporites may prime the tectonically involved successions for  
45 repeated dolomitization, and formation of potential reservoirs in sequential tectonic  
46 modifications (extensional vs. compressional).

## 47 **1 Introduction**

48 Fault-controlled dolomitization has been the focus of attention in many studies during the last  
49 decades due to its influential role in modifying the petrophysical properties of rocks and, hence,  
50 anisotropy in fluid migration pathways, and, ultimately on reservoir quality (e.g. Purser et al.,  
51 1994; Montanez, 1994; Zempolich and Hardie, 1997; Vandeginste et al., 2005; Davies and  
52 Smith, 2006; Sharp et al. 2010). The mechanical and hydrological behaviour of fault zones are in  
53 turn influenced by fluid-rock interactions and diagenetic modifications (e.g. Gale et al., 2004;  
54 Laubach et al., 2010; Clemenzi et al., 2015). It follows that the mutual interplay between fault  
55 activity and fluid-driven rock-fluid interaction can trigger dolomitization of carbonates and,  
56 consequently, variations in physico-chemical properties of fluids through time and space.  
57 Leaking or sealing behaviours of fault zones during deformation are key controls for fault-related  
58 fluid circulation. A detailed understanding of such an interplay is thus necessary to improve our  
59 capability of making reliable predictions of fault-related dolomitization in carbonate reservoirs.  
60 Studying outcrop analogues provides fundamental support to meet this requirement (e.g.  
61 Swennen et al., 2012; Dewit et al., 2014; Bistacchi et al., 2015).

62 The Lower Jurassic to Lower Cretaceous Umbria-Marche passive margin carbonate  
63 succession, in the Central Apennines (Italy), is intensely affected by localized dolomitization  
64 both in the onshore fold-and-thrust belt and in offshore foredeep and foreland areas (e.g. Murgia  
65 et al., 2004; Pierantoni et al., 2013). The dolomitized intervals are well-exposed in the core of the  
66 Montagna dei Fiori Anticline (~~e.g. Ronchi et al., 2003~~), where the dolomitized Lower Jurassic  
67 intervals (Calcare Massiccio, Bugarone and Corniola Formations) and their relationships with  
68 fault zones allow to study the mutual influence between deformation structures and dolomitized  
69 intervals (Fig. 1). These intervals, known as the Castel Manfrino Dolostones (Crescenti, 1969;  
70 Mattei, 1987; Koopman, 1983), have been previously studied by Ronchi et al. (2003) only at its  
71 reference section, exposed at the Castel Manfrino location (Fig. 1b), in the central sector of the  
72 Montagna dei Fiori Anticline (Fig. 2). A fault-controlled dolomitization model and the relative  
73 timing of dolomitization were proposed by ~~Ronchi (2003)~~the latter authors— based on the  
74 homogenization temperatures obtained from microthermometry of the fluid inclusions, and their  
75 relation with the thermal history of the studied area. However, no clear relation between  
76 dolomitization and structural evolution of the Montagna dei Fiori Anticline on a local scale was  
77 provided to confidently link the occurrence of dolomitization to a particular tectonic event.  
78 Moreover, the nature and origin of the dolomitizing fluids were not well constrained. Recent re-  
79 evaluation of dolostone distribution in the Montagna dei Fiori Anticline (Storti et al., 2017a),  
80 showed that the dimension of the dolomitized geobodies (Fig. 2) is much more significant than  
81 what was previously mapped by Mattei (1987). Dolostones are distributed within fault damage  
82 zones and in the laterally adjacent carbonate rocks, and in intersection areas between fault sets,  
83 for a total area in map view of more than 1.5 km<sup>2</sup> (Storti et al., 2017a).

84 The structural pattern of the Montagna dei Fiori Anticline documents the overprinting of  
85 extensional and contractional deformation along major fault zones. ~~Although challenging, the~~The  
86 preserved structural framework in this anticline provides an opportunity to study the direct but  
87 complex regional tectonic controls on dolomitization in carbonate successions undergoing  
88 multiple deformation events, from rifting to folding and thrusting. This contribution integrates  
89 field mapping, new petrographic, geochemical, and microthermometric analyses, with structural  
90 studies to characterize the temporal record of fault-controlled diagenetic phases and, more  
91 specifically, dolomitization in the carbonatic succession outcropping in the Montagna dei Fiori  
92 Anticline. Therefore provides insights into the structural controls on regional fluid flow and their

93 chemical evolution through time. These findings might be of relevance for exploration and  
94 reservoir quality prediction onshore and offshore the Apennines and Southern Alps. Moreover,  
95 this work provides additional evidence of the potential influence of fluids derived from  
96 evaporitic detachment levels in modifications of geochemical trends and petrophysical properties  
97 of the overlying carbonate rocks.

## 98 **2 Geological setting**

99 The Montagna dei Fiori Anticline is a NNW-SSE striking, thrust-related fold located at  
100 the mountain front of the Central Apennines (Fig. 1). The geodynamic evolution of the  
101 Apennines is generally known to be the result of the superposition of NE-SW compression (in  
102 present-day geographic coordinates), related to the convergence between Eurasia and Africa  
103 plates since Late Cretaceous times (Elter et al., 1975; Dewey et al., 1989; Patacca et al., 1992),  
104 on a rifting-related tectono-sedimentary architecture produced by Early Jurassic extension (e.g.,  
105 Centamore et al., 1971). In such a framework, the Central Apennines developed during Miocene  
106 to Plio-Pleistocene times (e.g. Parotto and Praturlon, 1975; Barchi et al., 1998; Mazzoli et al.,  
107 2002; Bollati et al., 2012).

108 The Central Apennines involves the Umbria-Marche succession, which essentially  
109 includes Triassic to Miocene carbonates and marls, covered by Miocene to Pliocene syn-  
110 orogenic clastic sediments (Fig. 1). The pre-orogenic succession, from bottom to top, includes  
111 Late Triassic evaporites, dolomites and limestones (~~of the Burano Formation~~), which the basal  
112 detachment runs within its evaporitic interval (Ghisetti and Vezzani, 2000), Early to Late  
113 Jurassic platform and basinal limestones and dolostones (Calcare Massiccio, Corniola, Rosso  
114 Ammonitico, Calcari a Posidonia and Calcari ad Aptici Formations), and Cretaceous to Early  
115 Miocene basinal carbonates (Maiolica, Marne a Fucoidi, Scaglia and Biscaro Formations). In  
116 general, the lower part of Burano Formation is overlaid by the fluvio-deltaic siliciclastics of the  
117 Verrucano Formation (Middle-Late Triassic) (Tongiorgi et al., 1977; Ghisetti and Vezzani, 2000;  
118 Tavani et al., 2008). Nevertheless, the existence of these siliciclastics in the Montagna dei Fiori  
119 area is not yet proved. Syn-orogenic deposits include Miocene marls and turbiditic sandstones  
120 (Marne con Cerroigna and Laga Formations) (Artoni, 2013 and references therein).  
121 The deposition of the Calcare Massiccio Formation, dated as Hettangian-Sinemurian and with a  
122 total thickness varying between 300 to 700 m (Pialli, 1971), records an important extension pulse  
123 in the evolution of Tethyan rifting. The following facies are observed in the lower part of the

124 Calcare Massiccio Formation: oncoïd-rich peloidal pack- to grainstones in alternation with  
125 peloidal wacke- to packstones including horizons of algal bindstones (Calcare Massiccio A;  
126 Brandano et al., 2016). The upper part is made up of beds of skeletal and coated grain wacke- to  
127 grainstones including microoncoïds, echinoderms, calcareous and siliceous sponges, bivalves,  
128 gastropods and ammonites (Calcare Massiccio B; Brandano et al., 2016). The lower part has  
129 been interpreted as having been deposited in a peritidal environment, while the upper part  
130 corresponds to lower to middle shelf depositional environments, characterized by a general  
131 deepening upward trend associated with extensional faulting and drowning of the platform,  
132 coupled with subsidence and deposition of the overlying Corniola Formation in the pelagic areas.  
133 Overall, the Early Jurassic rifting led to the growth of the Calcare Massiccio Formation in a  
134 carbonate platform setting, followed by faulting and drowning, and development of pelagic  
135 intrabasins filled by syn-rift sediments (Fig. 1c; Bernoulli et al. 1979; Santantonio and Carminati,  
136 2011). The syn-rift deposits include pelagic limestones of the Bugarone and Corniola  
137 Formations. Condensed pelagic limestones of the Bugarone Formation (Lower Pliensbachian-  
138 Lower Tithonian; Bugarone Group in Pierantoni et al., 2013) occur at the top of the Calcare  
139 Massiccio Formation where it formed fault-controlled highs marking the regional drowning of  
140 the carbonate platform (Santantonio and Carminati, 2011). While, the pelagic limestones of the  
141 Corniola Formation (Sinemurian-Toarcian; Colacicchi et al., 1975; Morettini et al., 2002;  
142 Bosence et al., 2009; Marino and Santantonio, 2010; Brandano et al., 2016) occur within the  
143 fault-controlled (half)grabens in lateral continuation with the Calcare Massiccio Formation. The  
144 Corniola Formation in the lower part consists of turbiditic lobes originated from tectonic  
145 brecciation of the Calcare Massiccio Formation, and at the upper part is a well-bedded pelagic  
146 mudstone with chert nodules (Di Francesco et al., 2010). ~~In the Montagna dei Fiori, the geologic~~  
147 ~~framework of the outcropping Calcare Massiccio Formation is still a matter of debate between a~~  
148 ~~fault-related tectonosedimentary pattern (Mattei, 1987; Storti et al., 2017b), and a gravity driven,~~  
149 ~~olistolith hypothesis (Di Francesco et al., 2010; Santantonio et al., 2017).~~ Recent  
150 detailed work in the Salinello valley (Storti et al., 2017a; 2018) documented that major outcrops  
151 of Calcare Massiccio are bounded by mostly ~ E-W and ~ N-S striking fault zones showing  
152 extensional kinematics and dominantly affecting the Jurassic rocks older than the Maiolica  
153 Formation (Fig. 2A2a, e.g. sites 1 to 4). Overprinting relations indicate that ~ E-W deformation  
154 structures are systematically younger than the ~ N-S ones. Similar trends were observed in syn-

155 rift fault zones in other anticlines of the Central Apennines (e.g. Cooper and Burbi, 1986;  
156 Alvarez, 1989; Chilovi et al., 2002). Such a tectonosedimentary inheritance was involved in the  
157 growth of the Montagna dei Fiori Anticline, which initiated during the Late Miocene (Mazzoli et  
158 al., 2002; Artoni, 2003) and progressively evolved into the upper thrust sheet of a well-  
159 developed antiformal stack until Plio-Pleistocene times (e.g. Ghisetti et al., 1993; Calamita et al.,  
160 1994; Artoni, 2013). A major structural feature trending parallel to the Montagna dei Fiori  
161 Anticline and dissecting it is the Montagna dei Fiori Fault, a NNW-SSE striking extensional fault  
162 system cutting at high angle through the folded footwall rocks, typically at the forelimb-crest  
163 transition (Figs. 1, 2). This fault consists of two partially overlapping main fault zones with an  
164 extensional stratigraphic separation exceeding 900 m, and ~~This fault system~~ juxtaposes intensely  
165 deformed Late Miocene sediments in the hanging wall, against dolomitized and undolomitized  
166 Lower Jurassic and Cretaceous limestones in the footwall (Figs. 1 and 2). The development of  
167 the Montagna dei Fiori Fault has been alternatively interpreted as either a pre- (e.g. Calamita et  
168 al., 1994, Mazzoli, 2002; Scisciani et al., 2002) or late-folding (Ghisetti and Vezzani, 2000)  
169 feature. More recently, the origin of the Montagna dei Fiori Fault has been ascribed to the mutual  
170 interaction between horizontal shortening and uplift, and episodic gravitational re-equilibration  
171 during antiformal stacking underneath the anticline during Plio-Pleistocene times (Storti et al.,  
172 2018).

### 173 **3 Methodology**

174 The stratigraphic and deformational features of dolostones were analyzed in more than 60  
175 outcrops. The distribution of dolomitized intervals as well as their cross-cutting relationships  
176 with bedding planes, stylolites, veins and structures were ground-truthed and  
177 sampled. For petrographic analyses, 130 polished thin sections were studied with standard  
178 petrographic methods (transmitted and UV-fluorescent light microscopy). Dolomite crystal  
179 morphology and texture is based on the classification proposed by Sibley and Gregg (1987).

180 The rock slabs and thin sections were stained using Alizarine Red S and potassium  
181 ferricyanide (Dickson, 1966) to discriminate dolomite from calcite and evaluate their iron  
182 content. Cold cathodoluminescence microscopy (CL) was carried out on representative thin  
183 sections (n = 80) at KU Leuven University (Belgium) using a Technosyn cathodoluminescence  
184 device (8-15 kV, 200-400  $\mu$ A gun current, 0.05 Torr vacuum and 5 mm beam width).

185  $\delta^{13}\text{C}$  and  $\delta^{18}\text{O}$  analysis were carried out on 117 samples. Powder samples (150 - 200  $\mu\text{g}$ )  
186 were obtained by applying a New Wave Research micromilling device and a dental drill at KU  
187 Leuven University (Belgium). The analysis was conducted at Parma University (Italy) and the  
188 Friedrich-Alexander-Universität (Erlangen-Nürnberg, Germany) laboratories using Finnigan  
189 DeltaPlus V and ThermoFinnigan 252 mass spectrometers, respectively. The carbonate powders  
190 were reacted with 100% phosphoric acid at constant temperature of 75°C. Several additional  $\text{CO}_2$   
191 reference gases (NBS18, NBS19, MAB99, and a pure Carrara marble) with known isotopic ratio  
192 were analyzed during the measurements to determine the  $\delta^{13}\text{C}$  and  $\delta^{18}\text{O}$  values of the sample.  
193 Reproducibility was checked by replicate analysis of laboratory standards and was better than  
194  $\pm 0.1\text{‰}$  for  $\delta^{13}\text{C}$  and  $\pm 0.2\text{‰}$  for  $\delta^{18}\text{O}$  at Parma University and  $\pm 0.04$  for  $\delta^{13}\text{C}$  and  $\pm 0.05\text{‰}$  for  
195  $\delta^{18}\text{O}$  at Friedrich-Alexander-Universität. Oxygen isotope composition of dolomites was  
196 corrected using the acid fractionation factors given by Rosenbaum and Sheppard (1986).  
197 Duplicate homogeneous samples measured in both labs for inter-laboratory reproducibility ~~show~~  
198  ~~$\delta^{13}\text{C}$  and  $\delta^{18}\text{O}$  values within the acceptable range of error deviation ( $\pm 0.1\text{‰}$ ) both for  $\delta^{13}\text{C}$  and~~  
199  ~~$\delta^{18}\text{O}$ .~~ All carbon and oxygen values are reported in per mil, relative to the “Vienna PDB scale”  
200 (V-PDB).

201 A total number of 21 samples were analyzed for their  $^{87}\text{Sr}/^{86}\text{Sr}$  ratios. The analyses were  
202 conducted at the Department of Analytical Chemistry, Ghent University (Belgium) and at the  
203 Vrije Universiteit Amsterdam (the Netherlands). NIST SRM 987 was used as the international Sr  
204 standard in both labs. At Ghent University, 15 sample powders (20 mg) were collected using a  
205 dental drill device. The  $^{87}\text{Sr}/^{86}\text{Sr}$  ratio measurements were performed using a Thermo Scientific  
206 Neptune Multi-collector Inductively Coupled Plasma Mass Spectrometer (MC-ICP-MS)  
207 instrument. Within the external precision, repeated analyses of the international Sr standard  
208 yielded an average  $^{87}\text{Sr}/^{86}\text{Sr}$  ratio of  $0.710271 \pm 0.000023$  (2SD,  $n = 43$ ), in agreement with the  
209 accepted  $^{87}\text{Sr}/^{86}\text{Sr}$  ratio of 0.710248 for this reference sample (Thirlwall, 1991). At Vrije  
210 Universiteit Amsterdam, 6 sample powders (2 - 3 mg) were collected using a New Wave  
211 Research micromilling device. Analyses were performed using a ThermoElectron Triton plus  
212 TIMS instrument. In order to monitor and document the system’s performance, repeated analyses  
213 of the international Sr standard ( $n = 58$ ) were carried out on load sizes of 10 ng and 100 ng which  
214 yielded average  $^{87}\text{Sr}/^{86}\text{Sr}$  ratios of  $0.710245 \pm 0.000022$  (2SD) and  $0.710242 \pm 0.000008$  (2SD),  
215 respectively. In both labs mass discrimination correction was performed via internal

216 normalization using Russell's exponential law and the accepted value (0.1194; Steiger and Jager,  
217 1977) of the invariant  $^{86}\text{Sr}/^{88}\text{Sr}$  ratio.

218 Fluid inclusion microthermometry analysis was performed on 11 doubly polished wafers  
219 (80-130  $\mu\text{m}$  in thickness). Measurements were carried out at Parma University (Italy) using  
220 Linkam THMSG-600 and Linkam MDS-600 heating-cooling stages coupled with a Leica DM  
221 2500 microscope. The stages were calibrated by synthetic Syn Fli<sup>TM</sup> fluid inclusion standards.  
222 A 100x objective was used during the microthermometry runs of the small inclusions. The  
223 microthermometry data were collected following the Fluid Inclusion Assemblage (FIA) approach  
224 described in Goldstein and Reynolds (1994) for carbonate minerals. The salinities are reported in  
225 equivalent weight percent NaCl (eq. wt. % NaCl) and were calculated based on the equation of  
226 Bodnar (1993).

227 In order to perform a high resolution petrography, Scanning Electron Microscope (SEM)  
228 and Back-scattered Scanning Electron Microscope (BSEM) analyses were conducted using a  
229 Jeol 6400 Scanning Electron Microscope (SEM) equipped with an Oxford EDS (Energy  
230 Dispersive System). Operating conditions were 15 kV and 1.2 nA, electron beam about 1  $\mu\text{m}$  in  
231 diameter and 100 s counting time; errors are  $\pm 2-5\%$  for major elements and  $\pm 5-10\%$  for minor  
232 components. The analysis focused mainly on detecting possible dolomite crystals inside the bed  
233 perpendicular stylolites affecting the Cretaceous Scaglia Formation.

## 234 **4 Results**

### 235 **4.1 Field observation and distribution of the dolomitized bodies**

236 Dolomitization affected the Calcare Massiccio, Bugarone and Corniola Formations.  
237 There is no evidences of dolomitization in the overlying and immediate surrounding successions  
238 (e.g. Maiolica and Scaglia Formations), though the base of Maiolica Formation is reported as  
239 dolomitized in the Central Apennines onshore (e.g. Pierantoni et al., 2013) and offshore areas  
240 (Murgia et al., 2004). Dolomitized intervals are folded in the forelimb of the Montagna dei Fiori  
241 Anticline and are abruptly truncated by the Montagna dei Fiori Fault, which juxtaposes them  
242 against intensely foliated Scaglia, Bisciario and Marne con Cerroigna Formations (Figs. 2 and 3).  
243 The distribution of dolomitized intervals is wider in the Salinello valley (Figs. [4B1b](#), [2A2a](#))  
244 perhaps due to a better exposure. In the Corano Quarry location, dolomitization occur in the  
245 Calcare Massiccio and Bugarone Formations only as meter-sized dolostone geobodies in the  
246 footwall of the Montagna dei Fiori Fault (Fig. 4).

247 Dolostone breccias in fault cores is typically clast-supported, with angular and  
248 millimeter- to centimeter-sized fragments (Fig. 3C), changing to crackle breccia (Woodcock and  
249 Mort, 2008) away from the master slip surface. In the proximity of the master slip surface,  
250 dolostone fragments are sporadically ~~overprinted~~cross-cut by millimeter-sized dolomite veins.  
251 The breccia fragments, where cemented, are commonly surrounded by calcite.

252 Dolomitization does not follow a systematic pattern. The lateral extend of dolomitization  
253 is gradual. In some outcrops, dolomitization fronts show irregular outlines following, but also  
254 cross-cutting, the bedding surfaces (Fig. 5). Dolomitized intervals vary in thickness from few  
255 meters to hundred meters affecting the totality of the exposed Calcare Massiccio and only the  
256 lower part of Corniola Formation, where no clay interlayers are present. Dolomitized intervals in  
257 the Corniola Formation have a darker color relative to the host rock and are systematically more  
258 fractured than the hosting limestone. High amplitude (> 1 mm) bed-parallel stylolites are clearly  
259 visible in both limestones and dolostones (Fig. 5). However, in some dolostones only ghosts of  
260 stylolite traces can be seen. The dolostones locally contain porosity, appearing as millimetre- to  
261 centimetre-sized pores.

## 262 4.2 Petrography

### 263 4.2.1 Early calcite cementation

264 The early diagenetic products in the studied intervals are generally non-ferroan calcite  
265 cements. The first calcite cements precipitated following a phase of bioclast micritization (*sensu*  
266 Bathurst, 1975) in grain supported intervals. In chronological order, they include: 1) fibrous  
267 cements (FC) riming the bioclasts, mostly in the peloidal facies of the Calcare Massiccio  
268 Formation (Fig. ~~6A6a~~). These cements are ~~dull~~dark brown to non-luminescent under  
269 cathodoluminescence; 2) mosaic cements (MC), commonly fill the intergranular pore spaces  
270 (Fig. ~~6B6b~~), and also occur as syntaxial overgrowths on echinoderm fragments. These cements  
271 exhibit deformation twinning and show well-developed ~~dull~~brown and orange concentric-  
272 zoned cathodoluminescence pattern (Figs. ~~6C-6c~~ and ~~Dd~~). They contain only mono-phase all-  
273 liquid inclusions. All of these cements are postdated by high amplitude bed-parallel stylolites.

### 274 4.2.2 Dolomitization

275 All the dolomite types are non-ferroan and dominantly fabric destructive. Dolomitization  
276 developed in all the facies types of the Calcare Massiccio and the overlying Bugarone

277 | Formations, but only at the lower part of the Corniola Formation which consists of resedimented  
278 | Calcare Massiccio breccias (turbiditic lobes). The two first dolomite types (D1 and D2) are the  
279 | dominant dolomite types in the studied outcrops. These dolomites are distributed within the  
280 | damage zones of the ~ N-S and E-W Jurassic rift-related extensional faults and, in places,  
281 | displaced by them (Fig. ~~2A2a~~, site 1). The third and fourth dolomite types (D3 and D4) are  
282 | mainly observed within the damage zone of the Montagna dei Fiori Fault (NNW-SSE), and  
283 | appear only as dolomitic pockets overprinting D1 and D2 at the proximity of the ~ N-S and E-W  
284 | extensional faults. The fifth dolomite type (D5) is found only within the brecciated zones  
285 | associated with the Montagna dei Fiori Fault damage zone. The distinctive petrographic features  
286 | of the recognized dolomite types are summarized below:

287 | **Dolomite 1 (D1)** is a replacive dolomite which commonly appears as dispersed rhombs and  
288 | aggregates, and locally rims fracture walls cemented by calcite (~~CV1~~) (Figs. ~~6E-6e~~ and ~~Ff~~). D1  
289 | postdates the micritic envelopes and early calcite cements, and predates high amplitude bed-  
290 | parallel stylolites (Figs. ~~6G-6g~~ and ~~Hh~~). The crystals are fine to medium sized (< 350 µm) ~~and~~  
291 | with planar-e and planar-s textures, consists-consisting of relatively turbid, solid-inclusion rich,  
292 | well-developed ~~euhedral to subhedral~~ crystals, ~~They show with~~ red luminescence, occasionally  
293 | developing a concentric zonation.

294 | **Dolomite 2 (D2)** is a replacive dolomite (Figs. ~~7A-7a~~ and ~~Bb~~), infrequently occluding existing  
295 | pore spaces. Like D1, it also ~~frequently~~ predates high amplitude bed-parallel stylolites (Figs. ~~6G~~  
296 | ~~6g~~ and ~~Hh~~). D2 generally exhibits a ~~tightly-closely~~ packed texture with no or little  
297 | intercrystalline porosity. The crystals are medium to coarse sized (≤ 500 µm) with planar-s to  
298 | non-planar textures. They including a turbid core followed by a transparent ~~subhedral to anhedral~~  
299 | rim and trace quantities of saddle dolomite developing swiping extinction. In some crystals one  
300 | additional turbid zone rich in solid and fluid inclusions is present. Cathodoluminescence  
301 | observations enabled to recognize the presence of D1 in their turbid cores. D2 crystals are  
302 | characterized by zones of bright red-pink luminescence separated by purple luminescence zones  
303 | (Fig. 7b).

304 | **Dolomite 3 (D3)** is present as small localized bodies in the Calcare Massiccio (at the Castel  
305 | Manfrino reference section), in the Corniola Formation (at the Osso Caprino Road), and in the  
306 | Calcare Massiccio and Bugarone Formations (at the Corano Quarry). In the Corano Quarry the  
307 | dolomitized Bugarone and Calcare Massiccio Formations are in the footwall of the Montagna dei

308 Fiori Fault; and juxtaposed to the undolomiteized, intensely foliated Scaglia Formation (the  
309 hanging wall). Within the Bugarone Formation in this fault damage zone, D3 locally cements the  
310 millimeter-sized angular breccias that are in turn affected by fault parallel stylolites (Figs. ~~7C-7c~~  
311 and ~~Dd~~). The SEM and BSEM analysis performed on the samples from the immediate adjacent  
312 Scaglia Formation within the aforementioned fault damage zone did not indicate the presence of  
313 any dolomite in this formation. D3 crystals are fine to medium sized (< 300 μm) mostly  
314 transparent euhedral to anhedral exhibiting planar-e to non-planar textures (< 300 μm), with  
315 minor development of saddle morphologies ~~in-of~~ larger crystals (> 500 μm) with planar-c texture  
316 (Figs. ~~7E-7e~~ to ~~Hh~~). The ~~euhedral to anhedral~~ replacive crystals ~~are generally replacive,~~  
317 displaying a faint core, which compared to previous dolomite types has fewer solid inclusions.  
318 The saddle crystals are occasionally replacive ~~but majorly appear as cement in fractures~~. They  
319 display typical curved and slightly serrated crystal terminations with swiping extinction. These  
320 saddle dolomites were only observed in the Castel Manfrino reference section. D3 generally  
321 exhibit a ~~dull-dark~~ purple color with bright orange zones and subzones in core and/or rims when  
322 viewed under cathodoluminescence (Figs. ~~7E-7e~~ to ~~Hh~~).

323 **Dolomite 4 (D4)** appears as a matrix replacive and dolomite cement surrounding porosity, and  
324 locally ~~recrystallizing-replacing~~ D1 and D2 (Figs. ~~8A-8a~~ to ~~Ff~~). D4 also occludes bed parallel  
325 shear fractures and appears along the bed parallel stylolites (Figs. ~~9A-9a~~ to ~~Dd~~). In the Castel  
326 Manfrino reference section, some intercrystalline vuggy porosity is filled with fine dolomite  
327 rhombs including D4 with relics of D2 within their core (Figs. ~~8E-8e~~ and ~~Ff~~). The porosity may  
328 be preserved or partially to completely filled by CV4. D4 crystals have a turbid, solid-inclusion  
329 rich core and transparent rim. They are fine to medium sized (< 200-350 μm), presenting  
330 subhedral-planar-s to-and infrequent ~~euhedral crystals~~ non-planar textures. D4 exhibits a distinct  
331 luminescence pattern including a purple zone and an irregular green subzone.

332 **Dolomite 5 (D5)** occurs as crystals cementing micro-veins that cross-cut precursor dolomite  
333 types including dolomitic breccia fragments. In cemented breccias, D5 is postdated by CV3. D5  
334 presents a planar-c texture is-transparent, anhedral and is characterized by a bright red  
335 luminescence (Figs. ~~9E-9e~~ and ~~Ff~~).

### 336 4.2.3 Late calcite cementation

337 Four generations of calcite veins postdating dolomitization have been identified (Figs. 10  
338 and 11): 1) Calcite vein 1 (CV1) occurs only in Calcare Massiccio limestones and is represented

339 | as centimeter-sized veins that their thickness does not exceed 1.5 cm. These veins are strata-  
340 | bound, bedding-perpendicular ~~veins~~ with irregular fracture walls, exhibiting white color in the  
341 | outcrops. They postdate the first dolomite type (D1) riming the same fractures that abut the high  
342 | amplitude bed parallel stylolites. CV1 often show blocky to elongated crystal morphologies and  
343 | displays well-developed deformation twinning planes (Type II of Burkhard, 1993). This calcite  
344 | exhibits concentric zonation and ~~dull-brown~~ zones alternate with orange luminescence zones  
345 | (Figs. ~~4A-11a~~ and ~~Bb~~). 2) Calcite vein 2 (CV2) exclusively occurs in the intensely deformed  
346 | Scaglia Formation within the fault damage zones and correspond to tension gashes associated  
347 | with stylolites (*sensu* Nelson, 1981). Their thickness does exceed 1 cm. They are often  
348 | discontinuous and branch to several microveins (thickness < 1mm) when their tips are not  
349 | intersected by stylolites. CV2 veins are mostly recorded in foliated shear deformation zones with  
350 | well-defined S-C fabrics, exhibiting blocky, elongated to fibrous shapes with strongly developed  
351 | tightly spaced deformation twinning planes (Type II of Burkhard, 1993). CV2 displays ~~yellow~~  
352 | brown to orange luminescence with locally darker sector zones. The ~~yellow-brown~~ to orange  
353 | luminescence characteristic of CV2 is comparable with those of encasing Scaglia host rocks  
354 | (Figs. ~~4C-11c~~ and ~~Dd~~). 3) Calcite vein 3 (CV3) occurs as cement, filling the extensional faults  
355 | master plane and isolated veins within ~~the extensional fault~~ their damage zones. These veins are  
356 | centimeter-sized with thicknesses of less than 2 cm. CV3 cements the brecciated fault-infillings  
357 | containing angular fragments of host rock limestones, dolostones and earlier calcites. In the  
358 | brecciated fault zones at the backlimb of the anticline (Montagna dei Fiori Fault), CV3 always  
359 | passively overgrows D5 in fractures and never cuts it. ~~postdates the last dolomitization phase~~  
360 | ~~(D5) with no evidence of physical disruption.~~ CV3 exhibits a translucent white ~~to translucent~~  
361 | color in hand specimen. The crystals are blocky with no or weakly developed deformation  
362 | twinning planes, and are characterized by a dark orange to brown luminescence with distinct  
363 | darker sector zones (Figs. ~~4E-11e~~ and ~~Ff~~). 4) Calcite vein 4 (CV4) exists as centimeter-sized  
364 | isolated veins, pore-filling as well as breccia cements postdating all the preceding dolomites and  
365 | calcites. The breccia fragments are more often dolostones. CV4 has a translucent white ~~to~~  
366 | ~~translucent white~~ color in hand specimen with blocky crystal morphology and no evidence of  
367 | subsequent deformation (e.g. deformation twinning planes), and is characterized by distinct  
368 | concentric zonation (Figs. ~~4G-11g~~ and ~~Hh~~).

### 369 | 4.3 Geochemistry

### 370 4.3.1 Carbon and oxygen stable isotopes

371 The carbon and oxygen stable isotopic data ( $\delta^{13}\text{C}$  and  $\delta^{18}\text{O}$ ) of host rocks, dolomites and  
372 calcites are given in Table 1 and shown in Figures [12A-12a](#) and [Bb](#). The marine stable isotopic  
373 compositions reported by Veizer et al. (1999) were used as marine reference values.  
374 Accordingly, Lower Jurassic marine limestones are characterized by  $\delta^{13}\text{C}$  values of -0.5 to  
375 +4.5‰ and  $\delta^{18}\text{O}$  values of -2.5 to +1.0‰ V-PDB. The  $\delta^{18}\text{O}$  values of the marine dolomites are  
376 known to be 3-4‰ V-PDB more enriched than those of co-genetic marine limestones (Land,  
377 1980; Major et al., 1992; Horita, 2014). Both  $\delta^{13}\text{C}$  and  $\delta^{18}\text{O}$  values of the host rocks are within  
378 the expected range of the Lower Jurassic marine limestones but the Corniola host rocks show  
379 slightly lower values comparing to those of Calcare Massiccio. In the Calcare Massiccio host  
380 rocks, the  $\delta^{13}\text{C}$  values plot between +2.4 and +3.1‰ and  $\delta^{18}\text{O}$  values are within the range of -1.6  
381 and 0.0‰ V-PDB. The  $\delta^{13}\text{C}$  values in the Corniola host rocks are +2.0 and +2.5‰ while the  
382  $\delta^{18}\text{O}$  values are -3.1 to -1.4‰ V-PDB. The  $\delta^{13}\text{C}$  and  $\delta^{18}\text{O}$  values of the Scaglia host rocks range  
383 between +1.0 to +3.3‰ for  $\delta^{13}\text{C}$  and -2.2 to -1.0‰ V-PDB for  $\delta^{18}\text{O}$ . The obtained values are  
384 characterized in the mean range of Upper Cretaceous to Paleogene marine limestones (Veizer et  
385 al., 1999; +1.0 to +4.5‰ for  $\delta^{13}\text{C}$  and -4.0 to +2.0‰ V-PDB for  $\delta^{18}\text{O}$ ).

386 The  $\delta^{13}\text{C}$  values of CV1 are between +1.6 and +2.1‰ which plot within the range of  
387 reference values (Jurassic) but are slightly lower than the surrounding host rock values. The  $\delta^{18}\text{O}$   
388 values are between -4.7 and -2.7‰ V-PDB which are lower than those of reference and host rock  
389 values.

390 The  $\delta^{13}\text{C}$  values of all dolomite types (+0.6 to +3.4‰) fall within the range of host rocks  
391 and Jurassic marine limestones (Veizer et al., 1999). The  $\delta^{18}\text{O}$  shows a wider range of values,  
392 somehow overlapping but also lower than ~~those of~~ host rocks (-4.5 to -0.9‰ V-PDB) and those  
393 expected for the ~~presumable~~ Lower Jurassic marine dolomites. The majority of values plot  
394 between -3.5 and -1.5‰ V-PDB. The small size and overgrowth nature of certain dolomite types  
395 (e.g. D2 and D5) limits their proper isolation for geochemical analyses. Only one sample from  
396 D1 dolomite could be measured for  $\delta^{13}\text{C}$  and  $\delta^{18}\text{O}$  values, showing +2.5 and -1.9‰ V-PDB,  
397 respectively. The  $\delta^{13}\text{C}$  and  $\delta^{18}\text{O}$  values of D3 dolomite range from +2.0 to +2.6‰ and -2.8  
398 to -1.9‰ V-PDB, respectively, with values lower than those of the host rock.

399 D4 dolomite has  $\delta^{13}\text{C}$  values between +2.4 and +2.5‰, and  $\delta^{18}\text{O}$  values of -3.0 to -2.5‰  
400 V-PDB. The  $\delta^{13}\text{C}$  and  $\delta^{18}\text{O}$  values of CV2 are +1.2 to +3.1‰ and -1.7 to -1.7‰ V-PDB,

401 respectively. The  $\delta^{13}\text{C}$  values of CV3 are between +0.5 and +2.4‰, and the  $\delta^{18}\text{O}$  values cover a  
402 range of -2.2 to 0.0‰ V-PDB. The  $\delta^{13}\text{C}$  and  $\delta^{18}\text{O}$  values of CV4 are +3.8 to +4.9‰ and -9.4  
403 to -9.1‰ V-PDB, respectively. The  $\delta^{13}\text{C}$  values are slightly higher but the  $\delta^{18}\text{O}$  values are  
404 considerably lower compared to preceding calcite generations and the measured values from host  
405 rocks.

#### 406 4.3.2 $^{87}\text{Sr}/^{86}\text{Sr}$ ratios

407 Samples from host rocks (i.e. Calcare Massiccio and Corniola Formations), dolomites  
408 (D1, D3 and D4) and the Scaglia Formation in juxtaposition with the dolostones were analyzed  
409 for their  $^{87}\text{Sr}/^{86}\text{Sr}$  isotopic ratios. The obtained ratios versus  $\delta^{18}\text{O}$  values of the analyzed samples  
410 are shown in Fig. 12C. The  $^{87}\text{Sr}/^{86}\text{Sr}$  ratios obtained from the Calcare Massiccio and Corniola  
411 limestones are 0.70766 and 0.70725 ( $n = 2$ ), respectively, which is in agreement with the values  
412 of the Lower Jurassic marine carbonates (0.70704-0.70768) reported by McArthur et al. (2012).  
413 CV1 show a value equal to 0.70773.

414 All the dolomite types display higher  $^{87}\text{Sr}/^{86}\text{Sr}$  ratios when compared to the host rocks  
415 and reference values of the Lower Jurassic marine carbonates. D1 (replacive) and D4 cements  
416 show a comparable narrow range with values between 0.70784 and 0.70790, respectively. ~~While,~~  
417 ~~the~~ The two D3 samples (replacive and cement) display higher  $^{87}\text{Sr}/^{86}\text{Sr}$  ratios (0.70858 and  
418 0.70963, respectively). The  $^{87}\text{Sr}/^{86}\text{Sr}$  ratios obtained for dolomites do not show co-variation with  
419 corresponding  $\delta^{18}\text{O}$  values. The radiogenic Sr analysis was not performed on D2 and D5 since  
420 the physical mixing with other dolomite types could not be avoided.

421 The  $^{87}\text{Sr}/^{86}\text{Sr}$  ratios of the two marly limestone samples of Scaglia Formation are 0.70784  
422 to 0.70790. The CV2 veins in Scaglia Formation show comparable ratios of 0.70779 and  
423 0.70787. These values fit within the limits of values assigned by McArthur et al. (2012) for the  
424 Cenomanian-Bartonian (Scaglia age) marine carbonates (0.70730-0.70790).

#### 425 4.4 Fluid inclusion microthermometry

426 The overview of microthermometry measurements is given in Table 1 and Figs. 13A to  
427 C. All the measured fluid inclusions are primary and occur in growth zones. Based on optical and  
428 fluorescence microscopy analysis of wafers all the inclusions are aqueous mono-phase (liquid)  
429 and two-phase (liquid and vapor) with relatively consistent L:V ratio of 10-15% within a single  
430 FIA (fluid inclusion assemblage).

431 | ~~On the basis of optical microscopy analysis of wafers,~~ D1 contain dominantly mono-  
432 phase aqueous inclusions with sizes greater than 5  $\mu\text{m}$ . It is common for small inclusions  
433 ( $< 3 \mu\text{m}$ ) to remain mono-phase all liquid at room temperature due to their metastability  
434 (Goldstein and Reynolds, 1994). Thus, to eliminate the possible role of metastability, the  
435 samples were placed in a freezer for several days following the procedures described in detail by  
436 Goldstein and Reynolds (1994). All liquid inclusions remained unchanged and no vapor bubble  
437 was developed within them, which discards the metastability effect. In order to properly observe  
438 | the phase transitions and determine the final melting temperature of ice in the all liquid  
439 inclusions, they were rapidly heated up to  $\sim 200^\circ\text{C}$  to stretch and nucleate a bubble at room  
440 temperature (Goldstein, 1990). All the inclusions froze at  $-65$  to  $-49^\circ\text{C}$ . The first melting ( $T_e$ )  
441 was detected between  $-22$  to  $-19.3^\circ\text{C}$ . The final ice melting ( $T_m$ ) appeared at temperatures  
442 between  $-7.7$  and  $-2^\circ\text{C}$ . Applying Bodnar's (1993) equation, the obtained final melting  
443 temperatures correspond to salinity ranges of 3.5 to 11.3 eq. wt. % NaCl.

444 D2 is characterized by the presence of mono-phase and infrequent two-phase inclusions  
445 generally within their growth zones. The homogenization temperature of two-phase inclusions  
446 varies between  $58$  and  $71^\circ\text{C}$ . Upon cooling, a complete freezing of the fluid phase is reached  
447 at  $-56$  to  $-40^\circ\text{C}$ . The first ice melting temperature was distinguished at  $-22^\circ\text{C}$ . The final ice  
448 melting temperatures fall within  $-17.5$  and  $-5^\circ\text{C}$ , corresponding to salinities between 7.9 and  
449 20.5 eq. wt. % NaCl.

450 D3 is commonly inclusion poor. The measureable inclusions were detected and examined  
451 only in saddle dolomite crystals. These crystals contain only two-phase aqueous inclusions. Their  
452 homogenization temperatures are within the narrow range of  $70$  to  $73^\circ\text{C}$ . The complete freezing  
453 and first ice melting temperatures could not be distinguished but the final ice melting  
454 temperature occurred at temperatures between  $-13$  and  $-6^\circ\text{C}$  equal to salinity ranges of 9.2 to  
455 16.9 eq. wt.% NaCl. The first melting temperatures of fluid inclusions in D1, D2 and D3 were  
456 about  $-21^\circ\text{C}$ , suggesting a  $\text{H}_2\text{O}$ -NaCl fluid system.

457 D4 contains only two-phase aqueous inclusions. The homogenization temperatures in D4  
458 vary between  $79$  and  $105^\circ\text{C}$ . Complete freezing of inclusions occurred at temperatures  
459 between  $-86$  and  $-54^\circ\text{C}$ . The first ice melting was detected at  $-35$  to  $-40^\circ\text{C}$  indicating the  
460 possible presence of divalent cations such as  $\text{Ca}^{2+}$  and/or  $\text{Mg}^{2+}$  in the fluids (Shepherd et al.,  
461 1985; Goldstein and Reynolds, 1994). The final ice melting temperatures fall within a range

462 of -15 and -9°C corresponding to salinities of 12.8 to 18.6 eq. wt. % NaCl. A couple of  
463 inclusions show homogenization temperatures exceeding 120°C with salinities higher than  
464 20 eq. wt. % NaCl. The inconsistent homogenization temperatures and salinities obtained for  
465 these fluid inclusions, within the framework of an individual fluid inclusion assemblage (FIA)  
466 described by Goldstein and Reynolds (1994), indicate possible re-equilibration of these  
467 inclusions and thus are not used in the interpretations.

468 The obtained homogenization temperatures in all fluid inclusion assemblages indicate the  
469 minimum temperatures at which the fluids could have been trapped (Goldstein and Reynolds,  
470 1994). No correction was made for pressure effects on entrapment temperatures since no data  
471 regarding the exact depth and pressure of entrapment are available. In absence of independent  
472 thermal indicators such as Conodont Alteration Index (CIA) and Vitrinite Reflectance (VR), the  
473 accuracy of pressure correction cannot be well constrained (Slobodník et al, 2006), and thus no  
474 correction was made for pressure effects on homogenization temperatures.

475 No measurable fluid inclusion could be identified in CV1 and CV2 due to intense  
476 deformation twinning. CV3 and CV4 contain only primary mono-phase aqueous inclusions,  
477 indicating an entrapment temperature of below about 40-50°C (Goldstein and Reynolds, 1994).  
478 A complete freezing of the inclusions in CV3 occurred at temperatures between -40 and -52.5°C.  
479 The first melting temperature was detected at about -21 to -22°C, suggesting a H<sub>2</sub>O-NaCl  
480 composition. The final melting temperatures range between -6.4 and -2.7°C, corresponding to  
481 salinities between 9.7 and 4.5 eq. wt. % NaCl. The majority of the values cluster between 7.8 and  
482 5 eq. wt. % NaCl.

483 The complete freezing temperatures of the inclusions in CV4 fall within -46 and -35.5°C.  
484 The first melting temperature could not be determined with confidence but the final melting  
485 temperatures were reached at about -0.1 to -1.8°C, corresponding to salinities of 0.17 to  
486 3.0 eq. wt. % NaCl.

## 487 **5 Discussion**

### 488 **5.1 Stable and radiogenic isotopic composition of the parental fluids**

489 The  $\delta^{13}\text{C}$  values of all dolomite types mimic the range of host rock and Jurassic marine  
490 limestones and, consequently, they can be interpreted as largely rock-buffered. Their  $\delta^{18}\text{O}$  values  
491 are partly comparable to those of their respective host rocks as well as Jurassic marine reference  
492 values but more depleted when compared to the presumable Jurassic marine dolomites. The

493 relatively depleted  $\delta^{18}\text{O}_{\text{dolomite}}$  values could indicate the contribution of heated fluids in  
494 dolomitization process, although it could also relate to recrystallization of a precursor dolomite  
495 by fluids at higher temperature or  $^{18}\text{O}$ -depleted (Land, 1980; 1985). The absence of distinctive  
496 textural evidence in the analyzed samples such as enlarged crystal size and/or systematic mottled  
497 cathodoluminescence pattern, and their co-variation with  $\delta^{18}\text{O}$  values do not confirm  
498 recrystallization (Mazzullo, 1992 and ref. therein). Nevertheless, special care was taken to avoid  
499 the samples that occasionally displayed scattered mottled luminescence.

500 The oxygen isotope fractionation relation between water and dolomite (Land, 1983) was  
501 used to determine the most plausible parental fluids. In order to avoid erroneous results due to  
502 rock-buffered  $\delta^{18}\text{O}$  values, only the  $\delta^{18}\text{O}$  values of dolomite cements, especially from the bed  
503 parallel veins containing D4 were used. These values may provide the closest approximation to  
504 the  $\delta^{18}\text{O}$  signature of the parental fluids (Barker and Cox, 2011). Accordingly, a  $\delta^{18}\text{O}$  value of  $\approx$   
505  $+2.5$  to  $+4\%$  V-SMOW was calculated for D3, while this values increase to  $\approx +5$  to  $+7.5\%$   
506 V-SMOW for D4 (Fig. 13D13d). ~~The calculated compositions of the potential parental fluids are~~  
507 ~~progressively higher~~—The higher  $\delta^{18}\text{O}$  composition of the dolomitizing fluids relative to the  
508 Mesozoic seawater, which is estimated at  $-1.2$  to  $-1\%$  V-SMOW (Shackleton and Kennett, 1975;  
509 Marshall, 1992; Saalen et al., 1996), is compatible with fluids derived from or that had interacted  
510 with siliciclastics, crystalline basement (Taylor, 1997) and/or evaporite-derived brines.

511 The  $^{87}\text{Sr}/^{86}\text{Sr}$  ratios obtained for all dolomite types are higher than the Lower Jurassic  
512 marine carbonate values (0.70704-0.70768; McArthur et al., 2012). Since marine carbonates  
513 have very low rubidium (Rb) concentrations they produce negligible *in situ* radiogenic  $^{87}\text{Sr}$  after  
514 their deposition (Stueber et al. 1972; Burke et al. 1982). Therefore, the higher  $^{87}\text{Sr}/^{86}\text{Sr}$  ratios can  
515 be explained by the contribution of fluids originated or interacted with potassium rich  
516 siliciclastics (K-feldspars), crystalline basement and/or stratigraphic levels with higher  $^{87}\text{Sr}/^{86}\text{Sr}$   
517 ratios (Emery and Robinson 1993; Banner, 2004). Taking into account that the Upper Triassic  
518 Burano Formation underlying the studied intervals as the basal detachment has  $^{87}\text{Sr}/^{86}\text{Sr}$  ratios  
519 between 0.70774 and 0.70794 (Boschetti et al., 2005), the  $^{87}\text{Sr}/^{86}\text{Sr}$  ratios (D1 and D4) can  
520 partially be explained by their contribution. However, this contribution cannot justify much  
521 higher  $^{87}\text{Sr}/^{86}\text{Sr}$  ratios recorded in D3, being higher than values reported for Phanerozoic  
522 seawater (McArthur et al., 2012), and the values recorded in adjacent basinal deposits (i.e.  
523 Corniola and Scaglia Formations). Therefore, parental fluids most likely originated from or had

524 interacted with the siliciclastics underlying the Burano Formation (Verrucano Formation), if  
525 present, and/or with the crystalline basement with common elevated  $^{87}\text{Sr}/^{86}\text{Sr}$  ratios (0.71500-  
526 0.72650; Del Moro et al., 1982). The lack of any ferroan diagenetic phase minimizes the  
527 intreaction of fluids produced by clay transformation/dewatering (i.e. smectite to illite  
528 transformation; Boles and Franks, 1979).

529 CV1 is characterized by  $\delta^{13}\text{C}$  and  $\delta^{18}\text{O}$  values lower than the host limestones (i.e. Calcare  
530 Massiccio), while its  $^{87}\text{Sr}/^{86}\text{Sr}$  ratio is comparable to them. The salinity and composition of the  
531 parental fluids cannot be inferred here since no measurable fluid inclusions were found within  
532 this cement. The  $^{87}\text{Sr}/^{86}\text{Sr}$  ratio being within the range of the corresponding host rocks and the  
533 reference values, points to a rock-buffered system for  $^{87}\text{Sr}/^{86}\text{Sr}$ .

534 The  $\delta^{13}\text{C}$  and  $\delta^{18}\text{O}$  values obtained for CV2, as well as  $^{87}\text{Sr}/^{86}\text{Sr}$  ratios, fall within the  
535 range of the Scaglia host rocks, thus reflecting their rock-buffered nature. This interpretation is  
536 further supported by the comparable luminescence characteristics of CV2 with that of encasing  
537 Scaglia host rocks. The fluids from which CV2 calcite precipitated, as expected for tension  
538 gashes, were most likely derived from carbonate dissolution during pressure-solution and  
539 stylolitization-, pointing to a closed fluid system in contrast with the subsequent vein generations.

540 CV3 is characterized by  $\delta^{13}\text{C}$  values within the Jurassic marine values but are generally  
541 lower than the host rocks, while their  $\delta^{18}\text{O}$  values partially overlap both the hosting limestones  
542 and dolostones. Microthermometry of fluid inclusions revealed only mono-phase aqueous  
543 inclusions and thus precipitation at relatively low temperature ( $\leq 40\text{-}50^\circ\text{C}$ ) with moderate  
544 salinity (4.5-9.7 eq. wt. % NaCl). Such levels of salinity can be assigned to evaporated seawater,  
545 residual brines or fluids derived from evaporite dissolution, and thus makes it difficult here to  
546 interpret their exact origin with the available data.

547 CV4 is the latest calcite phase, and records the  $\delta^{13}\text{C}$  and  $\delta^{18}\text{O}$  values, respectively  
548 enriched and significantly depleted when compared to their hosting rocks and preceding  
549 diagenetic products. Generally, the enrichment of  $^{13}\text{C}$  could suggest  $\text{CO}_2$  outgassing due to  
550 evaporation or pressure changes (Friedman, 1970; Hendry et al., 2015) or bacterial fermentation  
551 (methanogenesis) of organic matter (Hudson, 1977) in low temperature diagenetic environments.  
552 The homogenization temperature of CV4 being below about  $40\text{-}50^\circ\text{C}$  could support any of these  
553 processes. Their low  $\delta^{18}\text{O}$  values and fluid inclusions with salinities comparable to, but also

554 significantly lower than, seawater reflect the contribution of meteoric fluids during precipitation  
555 of this calcite.

## 556 **5.2 Origin of the dolomitizing fluids**

557 The contribution of brines that derived from highly evaporated seawater or evaporites is  
558 suggested by the elevated salinity values obtained from microthermometry of the fluid inclusions  
559 (3.5 to 20.5 eq. wt. % NaCl). Accordingly, two sources that could potentially provide such fluids  
560 can be proposed: 1) fluids related to the Late Messinian evaporites (Upper Miocene), associated  
561 with the overlying Laga Formation, ~~deposited during the Upper Miocene time,~~ and their possible  
562 downward percolation through fault zones by density driven flow and/or seismic pumping  
563 mechanisms (Sibson, 1981; McCaig, 1988, 1990); or their tectonic involvement into the  
564 Apenninic thrust wedge during its propagation (underthrusting; Lobato et al., 1983); and 2)  
565 fluids related to the underlying décollement-detachment horizon of the Burano evaporites (Upper  
566 Triassic) and their upward flow through fault zones during development of the Montagna dei  
567 Fiori Anticline. The first scenario is valid if the dolomitization would have occurred only from  
568 the Upper Miocene time onwards. Moreover, Several-several researchers (e.g. Vai and Ricci  
569 Lucchi, 1977; Bassetti et al., 1998; Roveri et al. 2001) have shown that the occurrence of  
570 primary shallow-water evaporites, which were dominantly gypsum, was limited only to the  
571 western and central parts of the northern Apennines consisting of thrust-top marginal basins. ~~In~~  
572 ~~contrast, evaporites never precipitated in parts of the central Apennines including the Montagna~~  
573 ~~dei Fiori region (Marche area)~~ (Roveri et al. 2001). Hence, the evaporitic horizons existing  
574 within the Laga Formation corresponds to re sedimentation (gypsum debris) of those previously  
575 precipitated in the marginal basins. This interpretation makes the Messinian evaporites an  
576 unlikely source of Mg-rich brines. Moreover, taking-Taking into account that the maximum  
577 burial related temperature of the Calcare Massiccio Formation did not exceed 80°C in the  
578 Montagna dei Fiori region (Ronchi et al., 2003), it's not likely that the downward percolation of  
579 relatively low-temperature brines derived from the Messinian evaporites, ~~located at the higher~~  
580 ~~stratigraphic levels,~~ could reach or exceed the high temperatures recorded in fluid inclusions of  
581 the studied dolomites ~~in the Calcare Massiccio Formation~~ (D4; up to 105°C), given that the  
582 homogenization temperatures reflect the minimum entrapment temperatures (Goldstein and  
583 Reynolds, 1994). Deep circulation of these brines, if existed, can also be excluded by their

584 | limited ~~tectonic~~ involvement within the thrust wedge being confined merely to the off shore  
585 | wards of the Montagna dei Fiori region (Artoni, 2013).

586 |         Accordingly, the Upper Triassic Burano Formation, the basal detachment, appears as the  
587 | most plausible source for the high salinity brines recorded in fluid inclusions, and likewise, the  
588 | Mg-rich fluids could have been originated from post-evaporite brines associated with them  
589 | (Carpenter, 1978; McCaffrey et al., 1987). The fluctuations in salinity may argue for ~~different~~  
590 | degrees of diverse range of fault connectivity, different degrees of rock-water interaction and  
591 | contribution of pore waters of lower salinity (e.g. marine or meteoric).

### 592 | **5.3 Timing and structural controls on the evolution of parental fluids**

593 |         A generalized paragenesis and the relative chronology of dolomitization in relation to the  
594 | structural evolution of the Montagna dei Fiori Anticline are illustrated in Figs. 14 and 15. The  
595 | paragenesis is constructed on the basis of direct evidences recorded during observations at  
596 | outcrop scale and microscopic observations (e.g. cross-cutting relationships between diagenetic  
597 | phases, stylolites, fractures and other structural kinematics), and indirect evidences (e.g. regional  
598 | geodynamics and burial history).

599 |         The occurrence of micritic envelopes and fibrous calcite cements (FC), in grain supported  
600 | stratigraphic levels of the Calcare Massiccio Formation, is interpreted to be of eogenetic origin  
601 | (i.e. marine phreatic diagenesis; Moore, 1989), reflecting an early diagenesis shortly after  
602 | deposition. The well-developed ~~dull brown~~ and orange concentric cathodoluminescence pattern  
603 | of the succeeding mosaic calcite cement (MC) suggests a progressive shift to more reducing  
604 | conditions during precipitation in a phreatic diagenetic environment (as shown in Li et al., 2017).  
605 | High amplitude bed parallel stylolites postdate both cements, which confirm their precipitation  
606 | before significant burial. The observations made here are in agreement with earlier work by  
607 | Giacometti and Ronchi (2000), interpreting that the Calcare Massiccio Formation was cemented  
608 | during the early diagenetic stages.

609 |         D1, CV1 and D2 are postdated by well-developed, high amplitude bed-parallel stylolites.  
610 | Presence of D1 and CV1 in bed-perpendicular veins typically abutted by these stylolites (see  
611 | Figs. ~~6E-6e~~ to Hh) support the interpretation that the first dolomitization event (D1 and D2) took  
612 | place before significant burial and stylolite development, ~~—, being —~~ The latter and bed-  
613 | perpendicular veins are dynamically compatible within the same stress field which is  
614 | characterized by a vertical, load-related maximum principal axis of the stress ellipsoid. The

615 dominantly mono-phase fluid inclusions within D1 and D2 are in agreement with precipitation  
616 temperatures below about 40-50°C, suggesting a relatively shallow to intermediate burial  
617 environment and hence supporting a pre-Apenninic orogeny age of precipitation from a mix of  
618 formational and extra-formational fluids with elevated  $^{87}\text{Sr}/^{86}\text{Sr}$  ratios. The distribution of D1  
619 and D2 localized nearby the rifting-related ~ N-S and E-W striking extensional faults and even  
620 their displacement along them (Fig. 2A2a, e.g. site 1), point to the possible contribution of these  
621 faults in occurrence of D1 and D2. These faults dominantly affect the Jurassic rocks older than  
622 the Maiolica Formation which is attributed to the post-rift deposits, therefore suggesting a pre-  
623 Maiolica age for these dolomite types. Although, an absolute age cannot be provided, based on  
624 the evidence discussed above, the circulation of Mg-rich fluids during this dolomitization event  
625 was most likely controlled by rifting-related Jurassic extensional fault zones cutting through the  
626 crystalline basement. Precipitation of D1 and D2 at the lower part of Corniola Formation which  
627 is known as the syn-rift deposit discards a pre-rift origin for these dolomites. The displacement  
628 of dolomites along the aforementioned faults is possibly related to their prolonged activation  
629 during Early to Late Jurassic. In addition to the role of these faults in channelizing the fluids,  
630 their mobilization must have been intensified by some deriving mechanisms. A thermal  
631 convection system derived from high hit flux during rifting was interpreted by Hollis et al.  
632 (2017) to be responsible for circulation of seawater in a syn-rift dolomitization case in the  
633 Hammam Faraun fault block (Suez Rift, Egypt). In such scenario, the salinity of the fluids and  
634 their  $^{87}\text{Sr}/^{86}\text{Sr}$  ratios are expected to be more or less within the range of seawater. Furthermore,  
635 this scenario seems unlikely in the studied area given the lack of a deep aquifer to accommodate  
636 the fault tips and promotes the lateral fluid flux from basin to the rift shoulders and vice versa.  
637 Taking into account that D1 and D2 are the volumetrically more relevant dolomites within the  
638 studied intervals, and assuming the likely role of syn-rift extensional faults (Early to Late  
639 Jurassic) in their precipitation, a dominantly syn-rift dolomitization process is proposed for the  
640 dolostones in the Montagna dei Fiori Anticline. Although, the CL zonation pattern observed in  
641 D2 may indicate changes in flow condition or fluid composition, the lack of physical disruptions  
642 such as multiple fracturing suggests external regional controls rather than slip along the same  
643 faults (Eichhubl and Boles, 2000). The absence of pervasive syn-dolomitization fracturing and  
644 brecciation as well as zebra fabrics in these dolomites, perhaps indicate a relatively calm tectonic  
645 period during dolomite development (e.g. Hollis et al., 2017).

646 D3 and D4 both record elevated  $^{87}\text{Sr}/^{86}\text{Sr}$  ratios which accounts for their fault-controlled  
647 origin. However, their occurrence at the top of the Calcare Massiccio and overlaying Bugarone  
648 Formation (Corano Quarry site) which is < 1 m thick in Montagna dei Fiori region, and is  
649 marked as the final rift deposit (Cardello and Doglioni, 2015) discards a syn-rift origin for these  
650 dolomites. Moreover, D3 and D4 postdate the development of high amplitude bed parallel  
651 stylolites. The formation of stylolites requires an approximate overburden of 600 to 1500 m  
652 (Lind, 1993; Machel, 1999; Mountjoy et al., 1999; Schulz et al., 2016), corresponding to a late to  
653 post-Maiolica deposition time (Early Cretaceous time onwards). The presence of D3 and D4  
654 dolomites in bed parallel fractures and shear veins (D4) suggests their association with  
655 contractional deformations, i.e. the most likely tectonic regime for explaining bed-perpendicular  
656 dilation. Therefore, the volumetrically minor second stage of dolomite precipitation may  
657 possibly be related to the Late- to post-Miocene compressional tectonics recorded in this region  
658 (e.g. Mazzoli et al., 2002; Artoni, 2013; Storti et al., 2018).

659 Dolostones containing D3 and D4 appear commonly as clast-supported breccias along  
660 fault zones pertaining to the Montagna dei Fiori Fault, then overprinted by fault-parallel  
661 stylolites. Accordingly, the occurrence of these dolomites was probably synchronous with the  
662 incipient stages of fault development, predating fault buttressing (Storti et al., 2018).  
663 Homogenization temperatures recorded in D4 (up to 105°C), much higher than the maximum  
664 temperatures recorded in the host rocks (below about 80°C; Ronchi et al., 2003), suggest  
665 hydrothermal fluid circulation. The development of the Montagna dei Fiori Anticline at the toe  
666 of the Late Miocene Central Apennines thrust wedge could have favored the forelandward  
667 migration of hydrothermal fluids expelled from the more internal regions of the belt, similarly to  
668 what has been proposed for the Rocky Mountains foreland (i.e. squeegee flow model; Machel  
669 and Cavell, 1999). Such a migration may have possibly favored the precipitation of D4 in bed  
670 parallel veins, generally considered as evidence for syn-compressional fluid overpressure  
671 (Sibson, 2001; Hiemstra and Goldstein, 2015). At this stage, in addition to dilation of the pre-  
672 existing ~ N-S and E-W striking rift-related extensional faults and their possible role in fluid  
673 migration, the excess of pore pressure at the base of the thrust ramp, in the fold hinge and during  
674 fold tightening could promote the localization of the fractures (Smith and Wiltschko, 1996;  
675 Ghisetti and Vezzani, 2000), with fluid migration within this zone and eventually dolomitization.  
676 These fractures could have been corridors that later on formed the insipient NW-SE Montagna

677 | dei Fiori Fault, and their localization at the back-limb cross-cutting the core, explaining best the  
678 | distribution of D3 and D4 at this locality. The presence of D5 only within the damage zone of the  
679 | Montagna dei Fiori Fault, postdating dolostone brecciation and, in places, cementing breccia  
680 | fragments, may suggest that D5 dolomite precipitation was associated with the late stage  
681 | evolution of the Montagna dei Fiori Fault, predating late stage calcite precipitation.

682 | The presence of several generations of bed perpendicular stylolites bounding and intersecting  
683 | CV2 veins, supports that late stage calcite cements precipitated closely associated with the  
684 | deformation history of the Scaglia Formation in the hanging wall of the Montagna dei Fiori  
685 | Fault, during buttressing against Calcare Massiccio and Corniola Formations in the footwall, and  
686 | related with the positive inversion event induced by thrust-sheet stacking at depth (Storti et al.,  
687 | 2018). Precipitation of CV3 and CV4 is interpreted to have occurred during uplift and cooling as  
688 | revealed by their relatively low homogenization temperatures ( $\leq 40\text{-}50^\circ\text{C}$ ). Deformation twinning  
689 | is either absent or weakly developed, reflecting the lack of significant tectonic deformation after  
690 | calcite precipitation. These cements postdate the dolomitization events, high amplitude bed  
691 | perpendicular and parallel stylolites, and are precipitated as cements bounding the breccia  
692 | fragments within the damage zone of the Montagna dei Fiori Fault. Salinities calculated from  
693 | their fluid inclusions, particularly in CV4 suggests precipitation from meteoric waters, which  
694 | should have been favored during the late evolutionary stages of antiformal stacking beneath the  
695 | Montagna dei Fiori Anticline, and eventual late extensional slip along the Montagna dei Fiori  
696 | Fault (Storti et al., 2018). The results obtained in this study are in relative agreement with the  
697 | earlier work by Ronchi et al. (2003) and Murgia et al. (2004) in the Central Apennines, assigning  
698 | dolomitization phases to the pre- and syn-orogenic deformations, although they did not specify  
699 | the direct relation between the local structures and the different types of dolomite.

700 | Although, the texture of the studied dolomites vary from planar-e to non-planar, the  
701 | preponderance of planar dolomite, as in D4, creates a rock with interesting poroperm  
702 | characteristics (e.g. Woody et al., 1996; Wilson et al., 2007; Wenzhi et al., 2012). This case-  
703 | study is certainly relevant for many potential reservoirs elsewhere in the world. Similar  
704 | multistage burial dolomitization events enhancing the reservoir quality have been reported from  
705 | the carbonate successions of the Jurassic in the Kopet-Dagh Basin, north eastern Iran (Adabi,  
706 | 2009) and Devonian of the Rainbow sub-Basin, western Canada (Qing and Mountjoy, 1989;  
707 | Lonnee, 1999).

708 **6 Conclusions**

709 The Lower Jurassic limestones outcropping at the core of the Montagna dei Fiori  
710 Anticline (Central Apennines, Italy) are massively affected by dolomitization, in damage zones  
711 of the pre-orogenic faults inherited from the Tethyan rifting and the ones formed during the  
712 Apenninic orogeny. Cross-cutting relationships between deformation structures, and results from  
713 optical and cold cathodoluminescence petrography, fluid inclusion microthermometry, and  
714 isotope geochemistry, support the occurrence of two major dolomitization events. The first event  
715 is interpreted as developed during the late stages of Tethyan rifting in Jurassic and resulted in  
716 volumetrically significant dolostone geobodies. These dolostones are majorly matrix replacive  
717 and their precipitation initiated prior to the significant burial as reflected in their cross-cutting  
718 relationship with bed parallel stylolites, and by homogenization temperatures in fluid inclusions  
719 that are dominantly below about 40-50°C. The second dolomitization event corresponds to  
720 volumetrically less relevant replacive dolomite and dolomite cements occluding fractures. These  
721 dolomites precipitated during hydrothermal fluid circulation associated with contractional  
722 tectonics during the Apenninic orogeny, possibly at the onset of the growth of the Montagna dei  
723 Fiori Anticline (Late Miocene).

724 Dolomitizing fluids in both events were most likely sourced from evaporitic brines  
725 associated to the underlying Burano evaporites and their interaction with siliciclastics and/or the  
726 crystalline basement.

727  
728 *Author contributions.* M. Mozafari participated in fieldwork, performed petrographic and  
729 microthermometric analyses, provided their interpretation, and wrote the manuscript; R.  
730 Swennen participated in fieldwork, discussed the results of the diagenetic study, and critically  
731 reviewed the manuscript; F. Balsamo contributed to collect and interpret structural data,  
732 discussed structural diagenesis data interpretation, and critically reviewed the manuscript; H. El  
733 Desouky collected  $^{87}\text{Sr}/^{86}\text{Sr}$  data; F. Storti conceived the research, contributed to collect and  
734 interpret structural data, discussed structural diagenesis data interpretation, and critically  
735 reviewed the manuscript; C. Taberner participated in fieldwork, discussed the results of the  
736 diagenetic study and their framing into the proposed structural evolution, and critically reviewed  
737 the manuscript.

738

739 *Acknowledgments.* This research was performed by collaboration between Parma and KU  
740 Leuven universities in the framework of a research project (PT12432 and GFSTE 1100942)  
741 funded by Shell Global Solutions International (Carbonate Research Team, now Geology and  
742 New Reservoir Types Team). We thank E.M. Selmo (Parma University) and M. Joachimski  
743 (University of Erlangen, Germany) for the stable carbon and oxygen analysis. G. Davis (VU  
744 Amsterdam, the Netherlands) is thanked for the strontium isotope analysis. A. Comelli and H.  
745 Nijs are kindly thanked for the careful preparation of the wafers and thin sections. L. Barchi is  
746 gratefully appreciated for his help in SEM analysis. We gratefully acknowledge A. Koopman for  
747 the constructive discussions during field work.

748

749 **References**

- 750 Adabi, M. H.: Multistage dolomitization of upper jurassic mozduran formation, Kopet-Dagh  
751 Basin, ne Iran. Carbonates and Evaporites, 24, 16-32,  
752 <https://doi.org/10.1007/BF03228054>, 2009.
- 753 Alvarez, W.: Evolution of the Monte Nerone Seamount in the Umbria-Marches Apennines; I,  
754 Jurassic-Tertiary stratigraphy, B. Soc. Geol. Ital., 108, 3-21, 1989.
- 755 Amieux, P.: La cathodoluminescence: méthode d'étude sédimentologique des carbonates, B.  
756 Cent. Rech. Explor.-Prod. Elf-Aquitaine, 6, 437-483, 1982.
- 757 Artoni, A.: Messinian events within the tectono-stratigraphic evolution of the Southern Laga  
758 Basin (Central Apennines, Italy), B. Soc Geol. Ital., 122, 447-466, 2003.
- 759 Artoni, A.: The Pliocene-Pleistocene stratigraphic and tectonic evolution of the central sector of  
760 the Western Periadriatic Basin of Italy, Mar. Pet. Geol., 42, 82-106,  
761 <https://doi.org/10.1016/j.marpetgeo.2012.10.005>, 2013.
- 762 Banner, J. L.: Radiogenic isotopes: systematics and applications to earth surface processes and  
763 chemical stratigraphy, Earth. Sci. Rev., 65, 141-194, [https://doi.org/10.1016/S0012-](https://doi.org/10.1016/S0012-8252(03)00086-2)  
764 [8252\(03\)00086-2](https://doi.org/10.1016/S0012-8252(03)00086-2), 2004.
- 765 Barchi, M., Minelli, G., and Piali G.: The CROP 03 profile: a synthesis of results of deep  
766 structures of the Northern Apennines, Mem. Soc. Geol. It., 52, 383-400, 1998.
- 767 Barker, S. L., and Cox, S. F.: Evolution of fluid chemistry and fluid-flow pathways during  
768 folding and faulting: an example from Taemas, NSW, Australia, Geol. Soc. London  
769 Spec. Publ., 359, 203-227, <https://doi.org/10.1144/SP359.12>, 2011.
- 770 Bassetti, M. A., Ricci Lucchi, F., Roveri, M., Taviani, M.: Messinian facies in a critical section  
771 of northern Apennines (Montepetra-Perticara, Pesaro), Giorn. Geol., 60, 261-263,  
772 1998.
- 773 Bathurst, R. G. C. (Eds.): Carbonate sediments and their diagenesis, Dev. Sedimentol., Ser.,  
774 Elsevier, 12, 658 pp., 1975.
- 775 Bathurst, R. G. C.: Deep crustal diagenesis in limestones: Revista del Instituto de Investigaciones  
776 Geologicas, Deputacion Provincial, Universidad Barcelona, 34, 89-100, 1980.
- 777 Bernoulli, D., Kálin, O., and Patacca, E.: A sunken continental margin of the Mesozoic Tethys:  
778 The Northern and Central Apennines, Symposium" Sédimentation jurassique W  
779 Européen", Spec. Publ. Ass. Sedim. Francis, 1, 179-210, 1979.

780 Bodnar, R. J.: Revised equation and table for determining the freezing point depression of H<sub>2</sub>O-  
781 NaCl solutions, *Geochim. Cosmochim. Acta*, 57, 683-684, 10.1016/0016-  
782 7037(93)90378-A, 1993.

783 Boles, J. R. and Franks, S. G.: Clay diagenesis in Wilcox Sandstone of southwest Texas:  
784 Implications of smectite diagenesis and sandstone cementation, *J. Sediment. Petrol.*,  
785 49, 55-70, <https://doi.org/10.1306/212F76BC-2B24-11D7-8648000102C1865D>,  
786 1979.

787 Bollati, A., Corrado, S., and Marino, M.: Inheritance of Jurassic rifted margin architecture into  
788 the Apennines Neogene mountain building: a case history from the Lucretili Mts.  
789 (Latium, Central Italy), *Int. J. Earth Sci.*, 101, 1011-1031,  
790 <https://doi.org/10.1007/s00531-011-0694-7>, 2012.

791 Bosence, D., Procter, E., Aurell, M., Kahla, A. B., Boudagher-Fadel, M., Casaglia, F., Cirilli, S.,  
792 Mehdie, M., Nieto, L., Rey, J., Scherreiks, R., Soussi, M., and Waltham, D.: A  
793 dominant tectonic signal in high-frequency, peritidal carbonate cycles? A regional  
794 analysis of Liassic platforms from western Tethys, *J. Sediment. Res.*, 79, 389-415,  
795 <https://doi.org/10.2110/jsr.2009.038>, 2009.

796 Boschetti, T., Venturelli, G., Toscani, L., Barbieri, M., and Mucchino, C.: The Bagni di Lucca  
797 thermal waters (Tuscany, Italy): an example of CaSO<sub>4</sub> waters with high Na/Cl and  
798 low Ca/SO<sub>4</sub> ratios, *J. Hydrol.*, 307, 270-293,  
799 <https://doi.org/10.1016/j.jhydrol.2004.10.015>, 2005.

800 Brandano, M., Cornacchia, I., Raffi, I., and Tomassetti, L.: The Oligocene-Miocene stratigraphic  
801 evolution of the Majella carbonate platform (Central Apennines, Italy), *Sediment.*  
802 *Geol.*, 333, 1-14, <https://doi.org/10.1016/j.sedgeo.2015.12.002>, 2016.

803 Burke, W. H., Denison, R. E., Hetherington, E. A., Koepnick, R. B., Nelson, H. F., and Otto, J.  
804 B.: Variation of seawater <sup>87</sup>Sr/<sup>86</sup>Sr throughout Phanerozoic time, *Geology*, 10, 516-  
805 519, [https://doi.org/10.1130/0091-7613\(1982\)10<516:VOSSTP>2.0.CO;2](https://doi.org/10.1130/0091-7613(1982)10<516:VOSSTP>2.0.CO;2), 1982.

806 Burkhard, M.: Calcite twins, their geometry, appearance and significance as stress-strain markers  
807 and indicators of tectonic regime: a review, *J. Struct. Geol.*, 15, 351-368,  
808 [https://doi.org/10.1016/0191-8141\(93\)90132-T](https://doi.org/10.1016/0191-8141(93)90132-T), 1993.

809 Calamita, F., Cello, G., Deiana, G., and Paltrinieri, W.: Structural styles, chronology rates of  
810 deformation, and time-space relationships in the Umbria-Marche thrust system

811 (central Apennines, Italy), *Tectonics*, 13, 873-881,  
812 <https://doi.org/10.1029/94TC00276>, 1994.

813 Cardello, G. L., and Doglioni, C.: From mesozoic rifting to Apennine orogeny: the gran Sasso  
814 range (Italy), *Gondwana Res.*, 27, 1307-1334,  
815 <https://doi.org/10.1016/j.gr.2014.09.009>, 2015.

816 Carpenter, B.: Origin and chemical evolution of brines in sedimentary basins, *Oklahoma Geol.*  
817 *Surv.*, 79, 60-77, <https://doi.org/10.2118/7504-MS>, 1978.

818 Centamore, E., Chiocchini, U., and Moretti, A.. Geologia della zona tra Acerenza e Avigliano  
819 (Prov. di Potenza), *Studi Geol. Camerti*, 1, 97-122,  
820 <http://dx.doi.org/10.15165/studgeocam-1462>, 1971.

821 Chilovi, C., De Feyter, A. J., Minelli, G., and Barchi, M. R.. Neogene strike-slip reactivation of  
822 Jurassic normal faults in the M. Nerone-M. Catria Anticline (Umbro-Marchean Apennines,  
823 Italy), *Boll. Soc. Geol. It.*, 121, 199-207, 2002.

824 Choukroune, P., Gapais, D., and Merle, O.: Shear criteria and structural symmetry, *J. Struct.*  
825 *Geol.*, 9, 525-530, [https://doi.org/10.1016/0191-8141\(87\)90137-4](https://doi.org/10.1016/0191-8141(87)90137-4), 1987.

826 Clemenzi, L., Storti, F., Balsamo, F., Molli, G., Ellam, R., Muchez, P., and Swennen, R.: Fluid  
827 pressure cycles, variations in permeability, and weakening mechanisms along low-  
828 angle normal faults: The Tellaro detachment, Italy, *Am. Assoc. Pet. Geol. Bull.*, 127,  
829 1689-1710, <https://doi.org/10.1130/B31203.1>, 2015.

830 Colacicchi, R., Passeri, L., and Pialli, G.: Evidences of tidal environment deposition in the  
831 Calcare Massiccio formation (Central Apennines-Lower Lias), in: *Tidal Deposits*,  
832 edited by: Ginsburg, R. N., Springer, Berlin, Heidelberg, Germany, 345-353,  
833 <https://doi.org/10.1007/978-3-642-88494-8>, 1975.

834 Cooper, J. C., and Burbi, L.: The geology of the central Sibillini Mountains, *Mem. Soc. Geol. It.*,  
835 35, 323-347, 1986.

836 Crescenti, U.: Serie stratigrafiche della serie calcarea dal Lias al Miocene nella regione  
837 Marchigiana Abruzzese: parte I and II, *Mem. Soc. Geol. It.*, 8, 155-420, 1969.

838 Davies, G. R., and Smith, L. B. J.: Structurally controlled hydrothermal dolomite reservoir  
839 facies: an overview, *Am. Assoc. Pet. Geol. Bull.*, 90, 1641-1690, 2006.

840 Del Moro, A., Puxeddu, M., Radicati di Brozolo, F., and Villa, I. M.: Rb-Sr and K-Ar ages of  
841 minerals at temperatures of 300-400°C from deep wells in the Larderello geothermal

842 field (Italy), *Contrib. Mineral. Petr.*, 81, 349-349,  
843 <https://doi.org/10.1007/BF00371688>, 1982.

844 Dewever, B., Swennen, R., and Breesch, L.: Fluid flow compartmentalization in the Sicilian fold  
845 and thrust belt: implications for the regional aqueous fluid flow and oil migration  
846 history, *Tectonophysics*, 591, 194-209, <https://doi.org/10.1016/j.tecto.2011.08.009>,  
847 2013.

848 Dewey, J. F., Helman, M. L., Turco, E., Hutton, D. H. W., and Knott, S. D.: Kinematics of the  
849 western Mediterranean, in: *Alpine Tectonics*, edited by: Coward, M. P., Dietrich, D.,  
850 Park, R. G., *Geol. Soc. London Spec. Publ.*, 45, 265-283,  
851 <https://doi.org/10.1144/GSL.SP.1989.045.01.15>, 1989.

852 Dewit, J., Foubert, A., El Desouky, H. A., Muchez, P., Hunt, D., Vanhaecke, F., and Swennen,  
853 R.: Characteristics, genesis and parameters controlling the development of a large  
854 stratabound HTD body at Matienzo (Ramales Platform, Basque-Cantabrian Basin,  
855 northern Spain), *Mar. Pet. Geol.*, 55, 6-25, [10.1016/j.marpetgeo.2013.12.021](https://doi.org/10.1016/j.marpetgeo.2013.12.021), 2014.

856 Dickson, J. A. D.: Carbonate identification and genesis as revealed by staining, *J. Sediment.*  
857 *Petrol.*, 36, 491-505, [https://doi.org/10.1306/74D714F6-2B21-11D7-](https://doi.org/10.1306/74D714F6-2B21-11D7-8648000102C1865D)  
858 [8648000102C1865D](https://doi.org/10.1306/74D714F6-2B21-11D7-8648000102C1865D), 1966.

859 Di Francesco, L., Fabbi, S., Santantonio, M., Bigi, S., and Poblet, J.: Contribution of different  
860 kinematic models and a complex Jurassic stratigraphy in the construction of a  
861 forward model for the Montagna dei Fiori fault-related fold (Central Apennines,  
862 Italy), *Geol. J.*, 45, 489-505, <https://doi.org/10.1002/gj.1191>, 2010.

863 [Eichhubl, P., and Boles, J. R.: Rates of fluid flow in fault systems; evidence for episodic rapid](#)  
864 [fluid flow in the Miocene Monterey Formation, coastal California, \*Am. J. Sci.\*, 300,](#)  
865 [571-600, doi: 10.2475/ajs.300.7.571, 2000.](#)

866 Elter, P., Giglia, G., Tongiorgi, M., and Trevisan, L.: Tensional and contractional areas in the  
867 recent (Tortonian to Present) evolution of the Northern Apennines, *B. Geofis. Teor.*  
868 *Appl.*, 17, 3-18, 1975.

869 Emery, D., and Robinson, A. (Eds.): *Inorganic Geochemistry: Applications to Petroleum*  
870 *Geology*, Blackwell Science, Oxford, United Kingdom, 101-128, 1993.

871 Fantoni, R., and Franciosi, R.: Tectono-sedimentary setting of the Po Plain and Adriatic foreland,  
872 *Rend. Lincei*, 21, 197-209, <https://doi.org/10.1007/s12210-010-0102-4>, 2010.

873 Flecker, R., De Villiers, S., and Ellam, R. M.: Modelling the effect of evaporation on the  
874 salinity- $^{87}\text{Sr}/^{86}\text{Sr}$  relationship in modern and ancient marginal-marine systems: the  
875 Mediterranean Messinian Salinity Crisis, *Earth Planet. Sci. Lett.*, 203, 221-233,  
876 10.1016/S0012-821X(02)00848-8, 2002.

877 Friedman, I.: Some investigations of the deposition of travertine from Hot Springs-I. The  
878 isotopic chemistry of a travertine-depositing spring, *Geochim. Cosmochim. Acta*, 34,  
879 1303-1315, [https://doi.org/10.1016/0016-7037\(70\)90043-8](https://doi.org/10.1016/0016-7037(70)90043-8), 1970.

880 Gale, J. F., Laubach, S. E., Marrett, R. A., Olson, J. E., Holder, J., and Reed, R. M.: Predicting  
881 and characterizing fractures in dolostone reservoirs: Using the link between  
882 diagenesis and fracturing, *Geol. Soc. London Spec. Publ.*, 235, 177-192,  
883 <https://doi.org/10.1144/GSL.SP.2004.235.01.08>, 2004.

884 Giacometti, A., and Ronchi, P.: Early Lias Carbonate Platform: Facies and Diagenesis Analogies  
885 between the Calcare Massiccio (Umbro-Marchean Apennines) and the Inici Fm.  
886 (Sicily Channel), *Mem. Soc. Geol. It.*, 55, 271-278, 2000.

887 Ghisetti, F., and Vezzani, L.: Detachments and normal faulting in the Marche fold-and-thrust belt  
888 (Central Apennines, Italy): inferences on fluid migration paths, *J. Geodyn.*, 29, 345-  
889 369, [https://doi.org/10.1016/S0264-3707\(99\)00057-5](https://doi.org/10.1016/S0264-3707(99)00057-5), 2000.

890 Ghisetti, F., and Vezzani, L.: Interfering paths of deformation and development of arcs in the  
891 fold-and-thrust belt of the central Apennines (Italy), *Tectonics*, 16, 523-536,  
892 <https://doi.org/10.1029/97TC00117>, 1997.

893 Goldstein, R. H., and Reynolds, T. J.: Systematics of Fluid Inclusions in Diagenetic Minerals,  
894 *Soc. Sediment. Geol., Short Course*, 31, 199 pp., 1994.

895 ~~Gregg, J. M.: On the formation and occurrence of saddle dolomite discussion, *J. Sediment.*  
896 *Petrol.*, 53, 1025-1033, 1983.~~

897 ~~Gregg, J. M., Shelton, K. L., Johnson, A. W., Somerville, I. D., and Wright, W. R.:  
898 Dolomitization of the Waulsortian limestone (lower Carboniferous) in the Irish  
899 Midlands, *Sedimentology*, 48, 745-766, <https://doi.org/10.1046/j.1365-3091.2001.00397.x>, 2001.~~

901 Habermann, D., Neuser, R. D., and Richter, D. K.: REE-activated cathodoluminescence of  
902 calcite and dolomite: high-resolution spectrometric analysis of CL emission (HRS-

903 CL), *Sediment. Geol.*, 101, 1-7, [https://doi.org/10.1016/0037-0738\(95\)00086-0](https://doi.org/10.1016/0037-0738(95)00086-0),  
904 1996.

905 Hendry, J. P., Gregg, J. M., Shelton, K. L., Somerville, I. D., and Crowley, S. F.: Origin,  
906 characteristics and distribution of fault-related and fracture-related dolomitization:  
907 Insights from Mississippian carbonates, Isle of Man, *Sedimentology*, 62, 717-752,  
908 <https://doi.org/10.1111/sed.12160>, 2015.

909 Hiemstra, E. J., and Goldstein, R. H.: Repeated injection of hydrothermal fluids into downdip  
910 carbonates: a diagenetic and stratigraphic mechanism for localization of reservoir  
911 porosity, Indian Basin Field, New Mexico, USA, *Geol. Soc. London Spec. Publ.*,  
912 406, 141-177, <https://doi.org/10.1144/SP406.1>, 2015.

913 [Hollis, C., Bastesen, E., Boyce, A., Corlett, H., Gawthorpe, R., Hirani, J. Rotevatn, A., and](#)  
914 [Whitaker, F.: Fault-controlled dolomitization in a rift basin. \*Geology\*, 45, 219-222,](#)  
915 [<https://doi.org/10.1130/G38s394.1>, 2017.](#)

916 Horita, J.: Oxygen and carbon isotope fractionation in the system dolomite-water-CO<sub>2</sub> to  
917 elevated temperatures, *Geochim. Cosmochim. Acta*, 129, 111-124,  
918 <https://doi.org/10.1016/j.gca.2013.12.027>, 2014.

919 Horvath, F.: Towards a mechanical model for the formation of the Pannonian basin,  
920 *Tectonophysics*, 226, 333-357, [https://doi.org/10.1016/0040-1951\(93\)90126-5](https://doi.org/10.1016/0040-1951(93)90126-5), 1993.

921 Hudson, J. D.: Stable isotopes and limestone lithification, *Geol. Soc. London*, 133, 637-660,  
922 <https://doi.org/10.1144/gsjgs.133.6.0637>, 1977.

923 Koopman, A.: Detachment tectonics in the central Apennines, Italy, Ph.D. thesis, Utrecht  
924 University, The Netherlands, 155 pp., 1983.

925 Land L. S.: The isotopic and trace element geochemistry of dolomite: the state of the art, in:  
926 *Concepts and Models of dolomitization*, edited by: Zenger D. H., Dunham J. B. and  
927 Ethington R. L., *Soc. Econ. Paleontol. and Mineral., Spec. Pub.*, 28, 87-110, 1980.

928 Land L. S.: The application of stable isotopes to studies of the origin of dolomite and to  
929 problems of diagenesis of clastic sediments, in: *Stable Isotopes in Sedimentary*  
930 *Geology*, edited by: Arthur M. A., *Soc. Econ. Paleontol. and Mineral, Short Course*,  
931 10, 4-1, 1983.

932 Land L. S.: The origin of massive dolomite. *Jour. Geol. Educ.*, 33, 112-125, 1985.

933 Laubach, S. E., Eichhubl, P., Hilgers, C., and Lander, R. H.: Structural diagenesis, *J. Struct.*  
934 *Geol.*, 32, 1866-1872, <https://doi.org/10.1016/j.jsg.2010.10.001>, 2010.

935 Li, Z., Goldstein, R. H. and Franseen, E. K.: Meteoric calcite cementation: diagenetic response to  
936 relative fall in sea-level and effect on porosity and permeability, Las Negras area,  
937 southeastern Spain, *Sediment. Geol.*, 348, 1-18,  
938 <https://doi.org/10.1016/j.sedgeo.2016.12.002>, 2017.

939 Lind, I. L., Berger, W. H., and Kroenke, L. W.: Stylolites in chalk from leg 130, Ontong Java  
940 Plateau, in: *Proceedings of the Ocean Drilling Program, scientific results*, 445-451,  
941 1993.

942 Lobato, L. M., Forman, J. M. A., Fazikawa, K., Fyfe, W. S., and Kerrich, R.: Uranium in  
943 overthrust Archean basement, Bahia, Brazil. *Canadian Mineral.*, 21, 647-654, 1983.

944 [Lonnee, J. S.: Sedimentology, dolomitization and diagenetic fluid evolution of the Middle](#)  
945 [Devonian Sulphur Point Formation, northwestern Alberta, Ph.D. thesis, University of](#)  
946 [Windsor, Canada, 133 pp., 1999.](#)

947 Luczaj, J. A., and Goldstein, R. H.: Diagenesis of the Lower Permian Krider Member, southwest  
948 Kansas, USA: fluid-inclusion, U-Pb, and fission-track evidence for reflux  
949 dolomitization during latest Permian time, *J. Sediment. Res.*, 70, 762-773,  
950 <https://doi.org/10.1306/2DC40936-0E47-11D7-8643000102C1865D>, 2000.

951 Machel, H. G.: Effects of groundwater flow on mineral diagenesis, with emphasis on carbonate  
952 aquifers, *Hydrol. J.*, 7, 94-107, <https://doi.org/10.1007/s100400050>, 1999.

953 Machel, H. G., Mason, R. A., Mariano, A. N., and Mucci, A.: Causes and emission of  
954 luminescence in calcite and dolomite, in: *Luminescence microscopy and*  
955 *spectroscopy : Qualitative and quantitative applications*, edited by: Barker, C. E., and  
956 Kopp, O. C, *Soc. Sediment. Geol., Short Course*, 9-25, 1991.

957 Machel, H. G., and Cavell, P. A.: Low-flux, tectonically-induced squeegee fluid flow, *Bull. Can.*  
958 *Petrol. Geol.*, 47, 510-533, 1999.

959 Major, R. P., Lloyd, R. M. and Lucia, F. J.: Oxygen isotope composition of Holocene dolomite  
960 formed in a humid hypersaline setting, *Geology*, 20, 586-588,  
961 [https://doi.org/10.1130/0091-7613\(1992\)020<0586:OICOHD>2.3.CO;2](https://doi.org/10.1130/0091-7613(1992)020<0586:OICOHD>2.3.CO;2), 1992.

962 Marchegiani, L., Deiana, G., and Tondi, E.: Tettonica pre-orogena in Appennino centrale, *Stud.*  
963 *Geol. Camerti*, 14, 211-228, <http://dx.doi.org/10.15165/studgeocam-807>, 1999.

- 964 Marino, M., and Santantonio, M.: Understanding the geological record of carbonate platform  
965 drowning across rifted Tethyan margins: Examples from the Lower Jurassic of the  
966 Apennines and Sicily (Italy), *Sediment. Geol.*, 225, 116-137,  
967 <https://doi.org/10.1016/j.sedgeo.2010.02.002>, 2010.
- 968 Marshall, J. D.: Climatic and oceanographic isotopic signals from the carbonate rock record and  
969 their preservation, *Geol. Mag.*, 129, 143-160,  
970 <https://doi.org/10.1017/S0016756800008244>, 1992.
- 971 Mattei, M.: Analisi geologico-strutturale della Montagna dei Fiori (Ascoli Piceno, Italia  
972 Centrale), *Geol. Romana*, 26, 327-347, 1987.
- 973 Mazzoli, S., Deiana, G., Galdenzi, S., and Cello, G.: Miocene fault-controlled sedimentation and  
974 thrust propagation in the previously faulted external zones of the Umbria-Marche  
975 Apennines, Italy, *EGU Stephan Mueller Spec. Publ. Ser.*, 1, 195-209, 2002.
- 976 Mazzullo, S. J.: Geochemical and neomorphic alteration of dolomite: a review, *Carbonates  
977 Evaporites*, 7, 21-37, <https://doi.org/10.1007/BF03175390>, 1992.
- 978 McArthur, J. M., Howarth, R. J., and Shields, G. A.: Strontium isotope stratigraphy, in: *The  
979 Geologic Time Scale 2012*, edited by: Gradstein, F. M., Ogg, J. G., Schmitz, M., and  
980 Ogg, G., Elsevier, 127-144, <https://doi.org/10.1016/C2011-1-08249-8>, 2012.
- 981 McCaffrey, M. A., Lazar, B., Holland, H. D.: The evaporation path of seawater and the  
982 coprecipitation of Br- and K<sub>p</sub> with halite, *J. Sediment. Res.*, 57, 928-937,  
983 <https://doi.org/10.1306/212F8CAB-2B24-11D7-8648000102C1865D>, 1987.
- 984 McCaig, A. M.: Deep fluid circulation in fault zones, *Geology*, 16, 867-870,  
985 [https://doi.org/10.1130/0091-7613\(1988\)016<0867:DFCIFZ>2.3.CO;2](https://doi.org/10.1130/0091-7613(1988)016<0867:DFCIFZ>2.3.CO;2), 1988.
- 986 McCaig, A. M., Wickham, S. M., and Taylor, H. P.: Deep fluid circulation in alpine shear zones,  
987 Pyrenees, France: field and oxygen isotope studies, *Contrib. Mineral. Petr.*, 106, 41-  
988 60, <https://doi.org/10.1007/BF00306407>, 1990.
- 989 Montanez, I. P.: Late diagenetic dolomitization of Lower Ordovician, upper Knox carbonates: A  
990 record of the hydrodynamic evolution of the southern Appalachian Basin, *Am.  
991 Assoc. Pet. Geol. Bull.*, 78, 1210-1239, 1994.
- 992 Moore, C. H. (Eds.): *Carbonate diagenesis and porosity*, *Dev. Sedimentol.*, 46, Elsevier Sci.  
993 Publ., Amsterdam, The Netherlands, 338 pp., 1989.

- 994 Morettini, E., Santantonio, M., Bartolini, A., Cecca, F., Baumgartner, P. O., and Hunziker, J. C.:  
995 Carbon isotope stratigraphy and carbonate production during the Early-Middle  
996 Jurassic: examples from the Umbria-Marche-Sabina Apennines (central Italy),  
997 *Paleog., Paleocl., Paleoec.*, 184, 251-273, [https://doi.org/10.1016/S0031-](https://doi.org/10.1016/S0031-0182(02)00258-4)  
998 [0182\(02\)00258-4](https://doi.org/10.1016/S0031-0182(02)00258-4), 2002.
- 999 Mountjoy, E. W., Machel, H. G., Green, D., Duggan, J., and Williams-Jones, A. E.: Devonian  
1000 matrix dolomites and deep burial carbonate cements: a comparison between the  
1001 Rimbey-Meadowbrook reef trend and the deep basin of west-central Alberta, *B. Can.*  
1002 *Petrol. Geol.*, 47, 487-509, 1999.
- 1003 Murgia, M. V., Ronchi, P., and Ceriani, A.: Dolomitization processes and their relationships with  
1004 the evolution of an orogenic belt (Central Apennines and peri-adriatic foreland,  
1005 Italy), *AAPG Hedberg series*, 1, 277-294, <https://doi.org/10.1306/1025695H13121>,  
1006 2004.
- 1007 Nelson, R. A: Significance of fracture sets associated with stylolite zones, *Am. Assoc. Pet. Geol.*  
1008 *Bull.*, 65, 2417-2425, 1981.
- 1009 Parotto, M., and Praturlon, A.: Geological summary of the Central Apennines, *Quad. Ric. Sci.*,  
1010 90, 257-311, 1975.
- 1011 Patacca, E., Sartori, R., and Scandone, P.: Tyrrhenian basin and Apenninic arcs: Kinematic  
1012 relations since late Tortonian times, *Mem. Soc. Geol. It.*, 45, 425-451,  
1013 <http://hdl.handle.net/11568/11610>, 1992.
- 1014 Pialli, G.: Facies di piana cotidale nel Calcare Massiccio dell'Appennino umbro marchigiano,  
1015 *Boll. Soc. Geol. It.*, 90, 481-507, 1971.
- 1016 Pierantoni, P., Deiana, G., and Galdenzi, S.: Stratigraphic and structural features of the Sibillini  
1017 Mountains (Umbria-Marche Apennines, Italy), *Ital. J. Geosci.*, 132, 497-520,  
1018 <https://doi.org/10.3301/IJG.2013.08>, 2013.
- 1019 Purser, B., Tucker, M. and Zenger, D.: Problems, progress and future research concerning  
1020 dolomites and dolomitization, in: *Dolomites: a Volume in Honour of Dolomieu*,  
1021 edited by: Purser, B., Tucker, M. and Zenger, D., *IAS Spec. Publ.*, 21, 3-20, 1994.
- 1022 [Qing, H., and Mountjoy, E. W.: Multistage dolomitization in Rainbow buildups, Middle](#)  
1023 [Devonian Keg River Formation, Alberta, Canada. \*J. of Sediment. Res.\*, 59, 114-126,](#)  
1024 <https://doi.org/10.1306/212F8F30-2B24-11D7-8648000102C1865D>, 1989.

- 1025 Radke, B. M., and Mathis, R. L.: On the formation and occurrence of saddle dolomite, J.  
1026 Sediment. Res., 50, 1149-1168, [https://doi.org/10.1306/212F7B9E-2B24-11D7-](https://doi.org/10.1306/212F7B9E-2B24-11D7-8648000102C1865D)  
1027 8648000102C1865D, 1980.
- 1028 Ronchi, P., Casaglia, F., and Ceriani, A.: The multiphase dolomitization of the Liassic Calcare  
1029 Massiccio and Corniola successions (Montagna dei Fiori, Northern Apennines, Italy),  
1030 Boll. Soc. Geol. It., 122, 157-172, 2003.
- 1031 Rosenbaum, J., and Sheppard, S. M.: An isotopic study of siderites, dolomites, and ankerites at  
1032 high temperatures, Geochim. Cosmochim. Acta, 50, 1147-1150,  
1033 [https://doi.org/10.1016/0016-7037\(86\)90396-0](https://doi.org/10.1016/0016-7037(86)90396-0), 1986.
- 1034 Roveri, M., Bassetti, M. A., and Lucchi, F. R.: The Mediterranean Messinian salinity crisis: an  
1035 Apennine foredeep perspective, Sediment. Geol., 140, 201-214,  
1036 [https://doi.org/10.1016/S0037-0738\(00\)00183-4](https://doi.org/10.1016/S0037-0738(00)00183-4), 2001.
- 1037 Saelen, G., Doyle, P., and Talbot, M. R.: Stable-isotope analyses of belemnite rostra from the  
1038 Whitby Mudstone Fm., England: Surface water conditions during deposition of a  
1039 marine black shale, Palaios, 11, 97-117, <https://doi.org/10.2307/3515065>, 1996.
- 1040 Santantonio, M, and Carminati, E.: Jurassic rifting evolution of the Apennines and Southern Alps  
1041 (Italy): Parallels and differences, Geol. Soc. Am. B., 123, 464-484,  
1042 <https://doi.org/10.1130/B30104.1>, 2011.
- 1043 Santantonio, M. and Muraro, C.: The Sabina Plateau, Palaeoescrapment, and Basin-Central  
1044 Apennines, 6th international symposium on the Jurassic system, General Field Trip  
1045 Guidebook, Palermo, Italy, 271-315, 2002.
- 1046 Santantonio, M., Fabbi, S., and Bigi, S.: Discussion on «Geological map of the partially  
1047 dolomitized Jurassic succession exposed in the central sector of the Montagna dei  
1048 Fiori Anticline, Central Apennines, Italy», Ital. J. Geosci., 136, 312-316,  
1049 <https://doi.org/10.3301/IJG.2017.04>, 2017.
- 1050 Schulz, H. M., Wirth, R., and Schreiber, A.: Organic-inorganic rock-fluid interactions in  
1051 stylolitic micro-environments of carbonate rocks: a FIB-TEM study combined with a  
1052 hydrogeochemical modelling approach, Geofluids, 16, 909-924,  
1053 <https://doi.org/10.1111/gfl.12195>, 2016.

- 1054 Scisciani V., Tavarnelli, E., and Calamita, F.: The interaction of extensional and contractional  
1055 deformations in the outer zones of the Central Apennines, Italy, *J. Struct. Geol.*, 24,  
1056 1647-1658, [https://doi.org/10.1016/S0191-8141\(01\)00164-X](https://doi.org/10.1016/S0191-8141(01)00164-X), 2002.
- 1057 Shackleton, N. J., and Kennett, J. P.: Paleotemperature History of the Cenozoic and the Initiation  
1058 of Antarctic Glaciation Oxygen and Carbon Isotope Analyses in DSDP Sites 277, 279,  
1059 and 281, *Initial reports of Deep Sea Drilling Project*, 29, 743-755, 1975.
- 1060 Sharp, I., Gillespie, P., Morsalnezhad, D., Taberner, C., Karpuz, R., Vergés, J., Horbury, A.,  
1061 Pickard, N., J. Garland, J., and Hunt, D.: Stratigraphic architecture and fracture-  
1062 controlled dolomitization of the Cretaceous Khami and Bangestan groups: an outcrop  
1063 case study, Zagros Mountains, Iran, *Geol. Soc. London Spec. Publ.*, 329, 343-396,  
1064 <https://doi.org/10.1144/SP329.14>, 2010.
- 1065 Shepherd, T., Rankin, A. H., and Alderton, D. H. M. (Eds.): *A Practical Guide to Fluid Inclusion*  
1066 *Studies*, Glasgow: Blackie, 239 pp., 1985.
- 1067 Sibley, D. F., and Gregg, J. M.: Classification of dolomite rock textures, *J. Sediment. Petrol.*, 57,  
1068 967-975, <https://doi.org/10.1306/212F8CBA-2B24-11D7-8648000102C1865D>,  
1069 1987.
- 1070 Sibson, R. H.: Fluid flow accompanying faulting: field evidence and models, *Earthquake*  
1071 *prediction: an international review*, AGU, 4, 593-603,  
1072 <https://doi.org/10.1029/ME004p0593>, 1981.
- 1073 Slobodník, M., Muchez, P., Kral, J., and Keppens, E.: Variscan veins: record of fluid circulation  
1074 and Variscan tectonothermal events in Upper Palaeozoic limestones of the Moravian  
1075 Karst, Czech Republic, *Geol. Mag.*, 143, 491-508,  
1076 <https://doi.org/10.1017/S0016756806001981>, 2006.
- 1077 Smith, R. E., Wiltschko, D. V.: Generation and maintenance of abnormal fluid pressures beneath  
1078 a ramping thrust sheet: isotropic permeability experiments, *J. Struct. Geol.*, 18, 951-  
1079 970, [https://doi.org/10.1016/0191-8141\(96\)00023-5](https://doi.org/10.1016/0191-8141(96)00023-5), 1996.
- 1080 Steiger, R., and Jäger, E.: Subcommittee on geochronology: convention on the use of decay  
1081 constants in geo and cosmo chronology, *Earth Planet. Sci. Lett.*, 36, 359-362,  
1082 [https://doi.org/10.1016/0012-821X\(77\)90060-7](https://doi.org/10.1016/0012-821X(77)90060-7), 1977.
- 1083 Storti, F., Balsamo, F., and Koopman, A.: Geological map of the partially dolomitized Jurassic  
1084 succession exposed in the core of the Montagna dei Fiori Anticline, Central

1085 Apennines, Italy, *Ital. J. Geosci.*, 136, 125-135, <https://doi.org/10.3301/IJG.2016.05>,  
1086 2017a.

1087 Storti F., Balsamo, F., and Koopman, A.: Reply to: discussion on «Geological map of the  
1088 partially dolomitized Jurassic succession exposed in the central sector of the  
1089 Montagna dei Fiori Anticline, Central Apennines, Italy» by Santantonio, M., Fabbi,  
1090 S. and Bigi, S., *Ital. J. Geosci.*, 136, 317-319, <https://doi.org/10.3301/IJG.2017.04>,  
1091 2017b.

1092 Storti, F., Balsamo F., Mozafari M., Koopman A., Swennen R. and Taberner C.: Syn-  
1093 contractional overprinting between extension and shortening along the Montagna dei  
1094 Fiori Fault during Plio-Pleistocene antiformal stacking at the Central Apennines  
1095 thrust wedge toe, *Tectonics*, <https://doi.org/10.1029/2018TC005072>, 2018.

1096 Stueber, A. M., Pushkar, P., and Baldwin, A. D., JR.: Survey of  $^{87}\text{Sr}/^{86}\text{Sr}$  ratios and total  
1097 strontium concentrations in Ohio stream and ground waters, *Ohio J. Sci.*, 72, 98-104,  
1098 1972.

1099 Sommer, S. E.: Cathodoluminescence of carbonates, 1. Characterization of cathodoluminescence  
1100 from carbonate solid solutions, *Chemical Geology*, 9, 257-273,  
1101 [https://doi.org/10.1016/0009-2541\(72\)90064-2](https://doi.org/10.1016/0009-2541(72)90064-2), 1972.

1102 Swennen, R., Dewit, J., Fierens, E., Muchez, Ph., Shah, M., Nader, F. H., Hunt, D.: Multiple  
1103 dolomitisation events along the Ranero fault (Pozalagua Quarry, BasqueCantabrian  
1104 Basin): episodic earthquake activity, *Sedimentology*, 59, 1345-1374,  
1105 <https://doi.org/10.1111/j.1365-3091.2011.01309.x>, 2012.

1106 Tavani, S., Storti, F., Salvini, F., and Toscano, C.: Stratigraphic versus structural control on the  
1107 deformation pattern associated with the evolution of the Mt. Catria anticline, Italy, *J.*  
1108 *Struct. Geol.*, 30, 664-681, <https://doi.org/10.1016/j.jsg.2008.01.011>, 2008.

1109 Taylor, H. P.: Oxygen and hydrogen isotope relationships in hydrothermal mineral deposits, In:  
1110 *Geochemistry of hydrothermal ore deposits*, edited by: Barnes, H. L., Wiley and  
1111 Sons, New york, 229-302, 1997.

1112 Thirlwall, M. F.: Long-term reproducibility of multicollector Sr and Nd isotope ratio analysis,  
1113 *Chemical Geology*, 94, 85-104, [https://doi.org/10.1016/S0009-2541\(10\)80021-X](https://doi.org/10.1016/S0009-2541(10)80021-X),  
1114 1991.

- 1115 Tongiorgi, M., Rau, A., and Martini, I. P.: Sedimentology of early-alpine, fluvio-marine, clastic  
1116 deposits (Verrucano, Triassic) in the Monti Pisani (Italy), *Sediment. Geol.*, 17, 311-  
1117 332, [https://doi.org/10.1016/0037-0738\(77\)90051-3](https://doi.org/10.1016/0037-0738(77)90051-3), 1977.
- 1118 Vai, G. B., and Ricci Lucchi, F.: Algal crusts, autochthonous and clastic gypsum in a  
1119 cannibalistic evaporite basin: a case history from the Messinian of northern  
1120 Apennines. *Sedimentology*, 24, 221-244, <https://doi.org/10.1111/j.1365-3091.1977.tb00255.x>, 1977.
- 1122 Vandeginste, V., Swennen, R., Gleeson, S. A., Ellam, R. M., Osadetz, K., and Roure, F.: Zebra  
1123 dolomitization as a result of focused fluid flow in the Rocky Mountains Fold and  
1124 Thrust Belt, Canada. *Sedimentology*, 52, 1067-1095, <https://doi.org/10.1111/j.1365-3091.2005.00724.x>, 2005.
- 1126 Vandeginste, V., Swennen, R., Gleeson, S. A., Ellam, R. M., Osadetz, K., and Roure, F.:  
1127 Geochemical constraints on the origin of the Kicking Horse and Monarch Mississippi  
1128 Valley-type lead-zinc ore deposits, southeast British Columbia, Canada, *Mineralium  
1129 Deposita*, 42, 913-935, <https://doi.org/10.1007/s00126-007-0142-6>, 2007.
- 1130 Veizer, J., Ala, D., Azmy, K., Bruckshen, P., Buhl, D., Bruhn, F., Carden, G. A. F., Diener, A.,  
1131 Ebner, S., Godderis, Y., Jasper, T., Korte, C., Pawellek, F., Podlaha, O. G., and  
1132 Strauss, H.:  $^{87}\text{Sr}/^{86}\text{Sr}$ ,  $\delta^{13}\text{C}$  and evolution of Phanerozoic seawater, *Chemical  
1133 Geology*, 161, 59-88, [https://doi.org/10.1016/S0009-2541\(99\)00081-9](https://doi.org/10.1016/S0009-2541(99)00081-9), 1999.
- 1134 Walker, G., Abumere, O. E., and Kamaluddin, B.: Luminescence spectroscopy of Mn<sup>2+</sup> rock-  
1135 forming carbonates, *Mineral. Mag.*, 53, 201-11, 10.1180/minmag.1989.053.370.07,  
1136 1989.
- 1137 [Wenzhi, Z., Anjiang, S., Suyun, H., Baomin, Z., Wenqing, P., Jingao, Z. and Zecheng, W.:  
1138 Geological conditions and distributional features of large-scale carbonate reservoirs  
1139 onshore China. \*Petrol. Explor. Develop.\*, 39, 1-14, \[https://doi.org/10.1016/S1876-3804\\(12\\)60010-X\]\(https://doi.org/10.1016/S1876-3804\(12\)60010-X\), 2012.](#)
- 1141 Wilson, A., and Ruppel, C.: Salt tectonics and shallow subsea floor fluid convection: models of  
1142 coupled fluid-heat-salt transport, *Geofluids*, 7, 377-386,  
1143 <https://doi.org/10.1111/j.1468-8123.2007.00191.x>, 2007.

1144 [Wilson, M. E. J., Evans, M. J., Oxtoby, N. H., Nas, D. S., Donnelly, T. and Thirlwall, M.:  
1145 Reservoir quality, textural evolution, and origin of fault-associated  
1146 dolomites. AAPB Bull., 91, 1247-1272, 2007.](#)

1147 Woodcock, N. H., and Mort, K.: Classification of fault breccias and related fault rocks, Geol.  
1148 Mag., 145, 435-440, <https://doi.org/10.1017/S0016756808004883>, 2008.

1149 [Woody, R. E., Gregg, J. M. and Koederitz, L. F.: Effect of texture on petrophysical properties of  
1150 dolomite: Evidence from the Cambrian-Ordovician of Southeastern Missouri. AAPG  
1151 Bull., 80, 119-131, 1996.](#)

1152 Zempolich, W. G., and Hardie, L. A.: Geometry of dolomite bodies within deep-water  
1153 resedimented oolite of the Middle Jurassic Vajont Limestone, Venetian Alps, Italy:  
1154 Analogs for hydrocarbon reservoirs created through fault-related burial  
1155 dolomitization, in: Reservoir quality prediction in sandstones and carbonates, edited  
1156 by: Kupecz, A., Gluyas, J., and Bloch, S., AAPG Mem., 69, 127-162, 1997.

1157

1158

1159

1160

1161

1162

### 1163 **Table captions**

1164 **Table. 1.** Stable carbon and oxygen isotopes,  $^{87}\text{Sr}/^{86}\text{Sr}$  ratios, and fluid inclusion  
1165 microthermometry data (not pressure corrected) of host rocks and diagenetic phases in the  
1166 Montagna dei Fiori Anticline. Stable carbon and oxygen isotopes values are expressed in  
1167 ‰ V-PDB and salinity values in eq. wt. % NaCl.

### 1168 **Figure captions**

1169 Fig. 1. **Aa)** Simplified regional map (modified after Ghisetti and Vezzani, 1997) showing the  
1170 tectonic outlines of the Central Apennines and the study area (rectangle). **Bb)** Schematic

1171 geological map of the Montagna dei Fiori Anticline showing the distribution of dolostones  
1172 (modified after Storti et al., 2017a). **€c**) Lithostratigraphical column of the successions exposed  
1173 in Montagna dei Fiori (modified after Mattei, 1987; Di Francesco et al, 2010; Storti et al., 2018).  
1174 Letter B stands for the Bugarone Formation. Lithologies are mentioned in the text. Note that the  
1175 thickness of the not-outcropping formations (Triassic evaporites and the crystalline basement) is  
1176 not to scale. **Đd**) Geological transect across present day Central Apennines and the Adriatic Sea  
1177 (modified after Fantoni and Franciosi, 2010) with vertical exaggeration of 2:1. The dashed  
1178 rectangle indicates the Montagna dei Fiori Anticline region.

1179  
1180 Fig. 2. **Aa, Bb**) Geological map of the central sector of the Montagna dei Fiori Anticline, and  
1181 cross-section oriented parallel (a-b) to the hinge line representing the tectono-stratigraphic  
1182 architecture of the faulted anticline (modified after Storti et al., 2017a). The stereonet (Schmidt  
1183 equal area projection lower hemisphere) provide the attitude of the extensional faults. The  
1184 locations of the corresponding field sites are indicated by ~~numbers~~**letters**. **c**) At this location, well  
1185 exposed N-S striking extensional fault zones offset the dolomitized Corniola Formation. The  
1186 fault zone is characterized by near-horizontal stylolites localized in the footwall damage zone (4  
1187 fault data). **d, e and f**) These locations consist of mostly ~ E-W striking extensional fault zones.  
1188 Particularly evident are the boundary fault zones delimiting Calcare Massiccio in the main horst  
1189 block (site d: 20 fault data; site e: 24 fault data; site f: 9 fault data). **g and h**) At these locations,  
1190 dip-slip slickenlines support major extensional movements related to the Montagna dei Fiori  
1191 Fault. Contractional deformation structures are preserved in the bed-perpendicular stylolites,  
1192 shear surfaces and tension gashes arranged as S-C arrays (site g: 21 fault data; site h: 14 fault  
1193 data). Equal area projection, lower hemisphere.

1194  
1195 Fig. 3. **Aa**) Field photograph showing the deformed Scaglia Formation in the hanging wall (HW)  
1196 and brecciated, dolomitized Calcare Massiccio Formation in the footwall (FW) of the Montagna  
1197 dei Fiori Fault. **Bb**) A hand specimen from the deformed Scaglia formation showing the intensity  
1198 of the pressure solutions (TS) and their abutting relationship with calcite veins (CV2). **€c**) A  
1199 transmitted light photomicrograph of the dolomitized, brecciated Calcare Massiccio Formation.  
1200 Note all the breccia fragments are composed of dolomite (D4 here).

1201

1202 Fig. 4. Field photographs (Corano Quarry) showing the field relations between dolostones, host  
1203 | limestones and the Montagna dei Fiori Fault: **Aa**) Panoramic view showing the spatial  
1204 | relationship between limestones and dolostones (orange) in the damage zone of the Montagna  
1205 | dei Fiori Fault (F). Note that the limestones and including dolostones of the Calcare Massiccio  
1206 | and Bugarone Formations on the footwall (FW) and marly limestones of the Scaglia Formation  
1207 | on the hangingwall (HW) are intensely deformed. **Bb**) Plan view of the Calcare Massiccio  
1208 | limestone in the footwall damage zone: intersected by calcite veins (CV1), dolomitized and  
1209 | affected by bed perpendicular stylolites (arrows). **Cc**) Distinct transition (dashed line) between  
1210 | dolomitized and undolomitized Calcare Massiccio limestone in the footwall damage zone.

1211

1212 | Fig. 5. Field photograph (**Aa**) and a simplified sketch (**Bb**) of a dolomitic pocket within the  
1213 | folded Calcare Massiccio (grey color) and their relation with bed parallel stylolites (hammer is  
1214 | 40 cm long).

1215

1216 | Fig. 6. **Aa**) Transmitted light image showing a micritic peloid rimmed by the fibrous cements  
1217 | (FC) which are followed by the mosaic cements (MC). **Bb**) Transmitted light image showing  
1218 | mosaic cements (MC) in a peloidal limestone over printed by high amplitude bed parallel  
1219 | stylolites (dotted white line). Note the core of some of the peloids is partially cemented as well.  
1220 | **Cc**, **Dd**) Respectively, transmitted light and corresponding cathodoluminescence image of FC  
1221 | and MC cements. **Ee**) Transmitted light photomicrograph showing D1 crystals rimming a  
1222 | fracture which is cemented by CV1. The fracture is in turn affected by a bed parallel stylolite. **Ff**)  
1223 | Cathodoluminescence image showing D1 scattered in the host rock and riming the fracture. **Gg**,  
1224 | **Hh**) Respectively, transmitted light and corresponding cathodoluminescence image showing part  
1225 | of a bed parallel stylolite (dotted white line) overprinting D1 and D2 crystals.

1226

1227 | Fig. 7. **Aa**, **Bb**) Photomicrographs of respectively, transmitted light and corresponding  
1228 | cathodoluminescence image showing the zoned rhombs of D2 with the remnants of D1 preserved  
1229 | in their cloudy core. The pore space is occluded by D4. **Cc**, **Dd**) D3 cementing angular breccia  
1230 | fragments of the Bugarone Formation in the damage zone of the Montagna dei Fiori Fault in the  
1231 | Corano Quarry site. Note the breccia is overprinted by a fault parallel bed perpendicular stylolite.  
1232 | **Ee**, **Ff**) Photomicrographs of respectively, transmitted light and corresponding

1233 cathodoluminescence image showing the euhedral to subhedral crystals of D3 developing a  
1234 | bright subzone and rim. **Gg, Hh**) D3 with a saddle crystal outline (SD) postdating calcite cements  
1235 (MC) and a zoned D2 crystal. The saddle morphology is outlined by a dotted white line.

1236  
1237 Fig. 8. Photomicrographs of respectively, transmitted light and corresponding  
1238 | cathodoluminescence image of dolomite types: **Aa, Bb**) The cross-cutting relationship between  
1239 D3 and D4. Note the presence of D3 within the core of dolomite crystals overgrown by D4. **Cc,**  
1240 **Dd**) Successions of dolomite types. Note the green CL color of D4 crystals. Typically,  
1241 luminescent dolomites are known to show yellow, orange to red colors (Machel et al., 1991).  
1242 Green luminescence in carbonates including dolomite have been attributed by a number of  
1243 researchers to the incorporation of three valent rare earth elements (REE) such as  $Dy^{3+}$  and  $U^{3+}$   
1244 as luminescence activators within their crystal lattice (Luczaj and Goldstein, 2000). Another  
1245 possibility is the emplacement of  $Mn^{2+}$ , with yellow luminescence, in  $Ca^{2+}$  sites with blue  
1246 luminescence in the dolomite crystal lattice instead of preferential incorporation in the  $Mg^{2+}$  site  
1247 (Sommer, 1972b; Amieux, 1982; Walker et al., 1989; Habermann et al., 1999). Accordingly,  
1248 non-stoichiometric, Ca-rich and poorly ordered dolomites may favor  $Mn^{2+}$  incorporation into  
1249 | their  $Ca^{2+}$  site. **Ee, Ff**) Vuggy porosity rimmed by D4 (green CL). Note the porosity is filled with  
1250 fine dolomite rhombs including traces of D2 in their core and D4 overgrowths.

1251  
1252 Fig. 9. Photomicrographs showing respectively, transmitted light and corresponding  
1253 | cathodoluminescence image of D4 and D5 in relation to stylolites and fracturing: **Aa, Bb**) D4,  
1254 exploiting a bed parallel stylolite that crossed-cuts D1 and D2. **Cc, Dd**) A sub-horizontal fracture  
1255 cemented by D4. **Ee, Ff**) D5 microveins (arrows) intersecting all the predating dolomite types in  
1256 the footwall brecciated zone of the Montagna dei Fiori Fault.

1257  
1258 Fig. 10. Field photographs showing the major calcite vein settings observed in Montagna dei  
1259 | Fiori: **Aa**) Cross-sectional view of bed normal Calcite vein 1 (CV1) abutting bed parallel  
1260 stylolites in folded beds of the Calcare Massiccio Formation. **Bb**) Plan view of the Calcite vein 2  
1261 (CV2) intensely affecting the deformed Scaglia (Rossa) Formation. **Cc, Dd**) Cross-sectional view  
1262 of the Scaglia Formation, intensely affected by pressure solution seams of tectonic origin

1263 crossed-over by populations of bed-perpendicular Calcite veins (CV3) in an echelon extensional  
1264 arrays.

1265  
1266 Fig. 11. **Aa**) Cathodoluminescence and transmitted light (in set) image showing blocky to  
1267 elongated crystals of CV1 with zoned CL pattern. **Bb**) Transmitted light image showing intensely  
1268 twinned CV1 crystals overprinted by euhedral to subhedral crystals of D3. Photomicrographs of  
1269 respectively, transmitted light and corresponding cathodoluminescence image: **Cc**, **Dd**) CV2 in  
1270 the Scaglia Formation abutted by a bed perpendicular stylolite (indicated by white arrows and  
1271 dashed line). The crystals display blocky to fibrous morphologies, deformation twinning, and a  
1272 similar orange luminescence pattern comparable with the adjacent host rock. **Ee**, **Ff**) CV3  
1273 cementing the breccia fragments in the damage zone of the Montagna dei Fiori Fault. The  
1274 crystals are blocky and show faint deformation twinning. They are brown-orange with distinct  
1275 darker luminescence sector zones. **Gg**, **Hh**) CV4 present as a cement within a polygonal pore  
1276 space rimmed by dolomite. Note the blocky crystals, absence of deformation twinning and  
1277 distinct concentric luminescence zonation pattern. CV4 is corroded and followed by a late  
1278 telogenetic calcite.

1279  
1280 Fig. 12. **A, B**) Overview of the  $\delta^{13}\text{C}$  and  $\delta^{18}\text{O}$  values of dolomites (**Aa**) host rocks from  
1281 Montagna dei Fiori as well as calcite veins (**Bb**). The stable isotope value of Lower Jurassic  
1282 marine limestones based on Veizer et al. (1999) is indicated by a dashed rectangle in subset B.  
1283 The  $\delta^{18}\text{O}$  values of the marine dolomites are considered to be 3-4‰ V-PDB higher than those of  
1284 marine limestones (Land, 1980; Major et al., 1992; Horita, 2014). **Cc**) Cross-plot of  $^{87}\text{Sr}/^{86}\text{Sr}$   
1285 ratios and corresponding  $\delta^{18}\text{O}$  values of host rocks, dolomites and calcite veins compared with  
1286 Lower Jurassic marine carbonates  $^{87}\text{Sr}/^{86}\text{Sr}$  (dashed rectangle) framework reported by McArthur  
1287 et al. (2012).

1288  
1289 Fig. 13. Overview of microthermometry analysis of primary inclusions in Montagna dei Fiori:  
1290 **Aa**) Frequency distribution of the  $T_{\text{mice}}$  (°C) in dolomite phases. **Bb**) Frequency distribution of  
1291 the Th (°C) in dolomite phases. **Cc**) Salinity (eq. wt. % NaCl) versus Th (°C) of dolomite and  
1292 calcite phases. **Dd**) Isotopic fractionation diagram from Land (1983) used to determine the

1293 isotopic composition (‰ V-SMOW) of parental fluids in equilibrium with dolomites in  
1294 Montagna dei Fiori.

1295

1296 | Fig. 14. **A)** Generalized paragenesis of diagenetic phases in relation to deformational stages and  
1297 burial history of the Calcare Massiccio Formation in the Montagna dei Fiori Anticline. The  
1298 deformational stages are from Storti et al. (2018), and the burial curve is based on Ronchi et al.  
1299 | (2003). The burial curve was made based on paleo-depth, paleo-temperatures, sedimentation rate  
1300 and paleo- heat flow.

1301

1302 Fig. 15. Sketch showing the successive fault-related diagenetic phases, of most importantly  
1303 dolomitization, recorded in the carbonate succession exposed at the core of the Montagna dei  
1304 | Fiori Anticline (not scaled). Different diagenetic phases are indicated with different colors. **Aa)**  
1305 The first dolomitization event is pre-orogenic (syn-rift), triggered from the fluids channelized  
1306 along Jurassic extensional faults. This event occurred during burial compaction and development  
1307 of bed parallel stylolites (BS). It is represented by scattered dolomite rhombs (D1) followed by  
1308 calcite cementation (CV1). The dolomitization continued with precipitation of larger crystals of  
1309 | D2. **Bb)** Second dolomitization event: syn-orogenic (early folding/ faulting) dolomitization from  
1310 fluids that migrated from more internal regions of the thrust belt and were channelized along the  
1311 basal detachment level into the fold core. This dolomitization event presents matrix replacive and  
1312 cements displaying infrequent saddle outlines (SD) in pore spaces, within bed parallel veins and  
1313 shear fractures. These dolostones postdate compaction but are affected by bed perpendicular  
1314 stylolites (TS) generated by horizontal to sub-horizontal layer parallel shortening related to the  
1315 | growth of the Montagna dei Fiori Anticline. **Cc)** Extensional collapse of the anticline and  
1316 development of the Montagna dei Fiori Fault, followed by buttressing of the Scaglia against  
1317 Calcare Massiccio and Corniola Formations during positive inversion induced by continuing  
1318 underthrusting at depth. Precipitation of D5 in micro-veins and cements in breccia zones,  
1319 followed by late stage calcite cementation in the Montagna dei Fiori Fault damage zone (CV2,  
1320 CV3 and CV4).

	Stable isotopes		Sr isotopes	Fluid inclusion microthermometry		
	$\delta^{13}\text{C}$	$\delta^{18}\text{O}$	$^{87}\text{Sr}/^{86}\text{Sr}$	Th ( $^{\circ}\text{C}$ )	Salinity	n
Calcare Massiccio Fm.	+2.4 to +3.1	-1.6 to 0.0	0.70766	-	-	
Corniola Fm.	+2.0 to +2.5	-3.1 to -1.4	0.70725	-	-	
Scaglia Fm.	+1.0 to +3.1	-2.2 to -1.0	0.70784-0.70791	-	-	
D1	+2.5	-1.9	0.70789	$\leq 40-50$	3.5 to 11.3	<u>27</u>
CV1	+1.6 to +2.1	-4.7 to -2.7	0.70773	-	-	-
D2	-	-	-	$\leq 40-50$ to 71	7.9 to 20.5	<u>37</u>
D3	+2.0 to +2.6	-2.8 to -1.9	0.70859-0.70964	70 to 73	9.2 to 16.9	<u>9</u>
D4	+2.4 to +2.5	-3.0 to -2.5	0.70790	79 to 105	12.8 to 18.6	<u>7</u>
CV2	+1.2 to +3.1	-1.7 to -1.6	0.70779 - 0.70787	-	-	
CV3	+0.5 to +2.4	-2.2 to 0.0	-	$\leq 40-50$	4.5 to 9.7	<u>9</u>
CV4	+3.8 to +4.9	-9.4 to -9.1	-	$\leq 40-50$	0.17 to 3.0	<u>19</u>

Table. 1

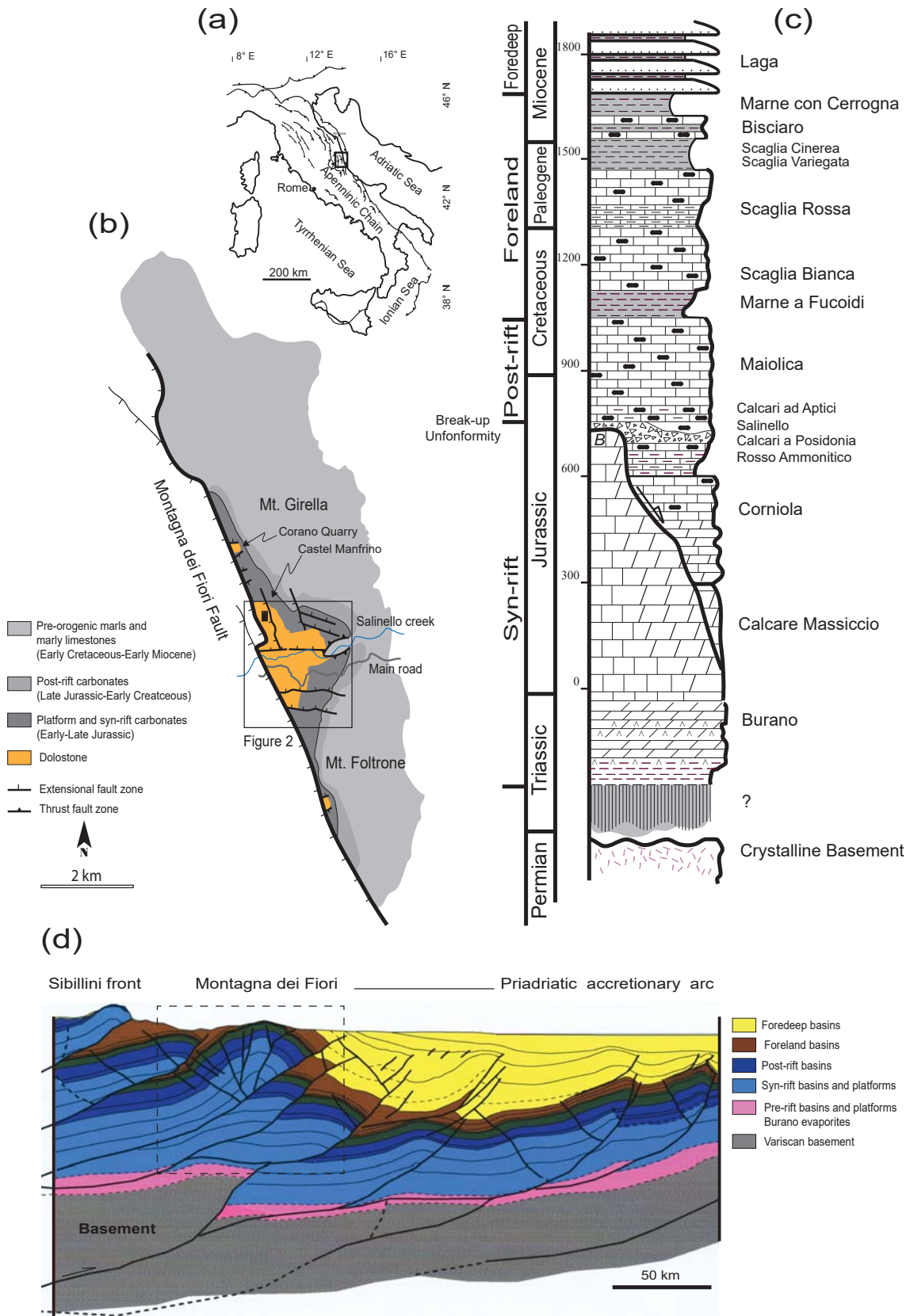


Fig. 1

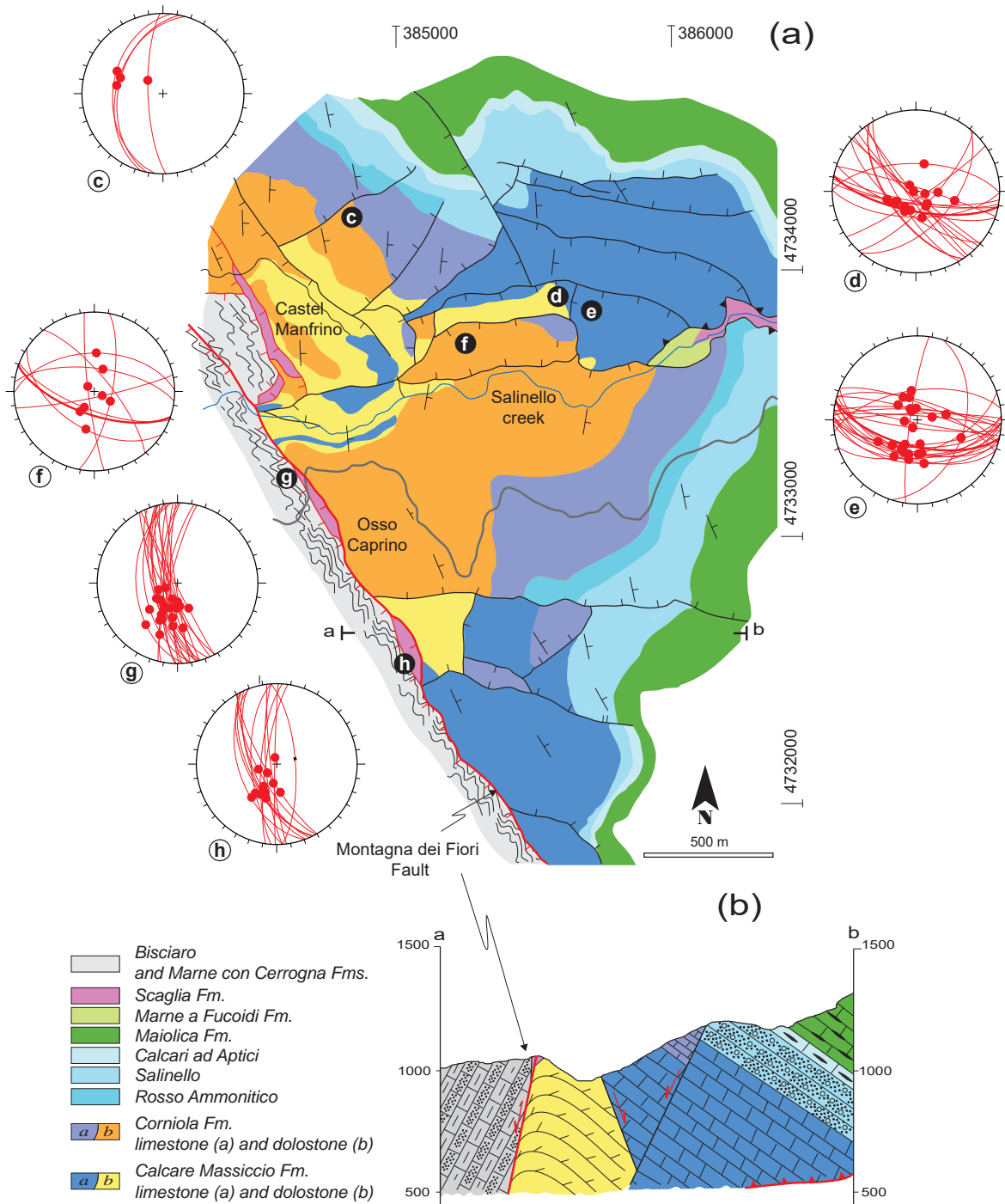


Fig. 2

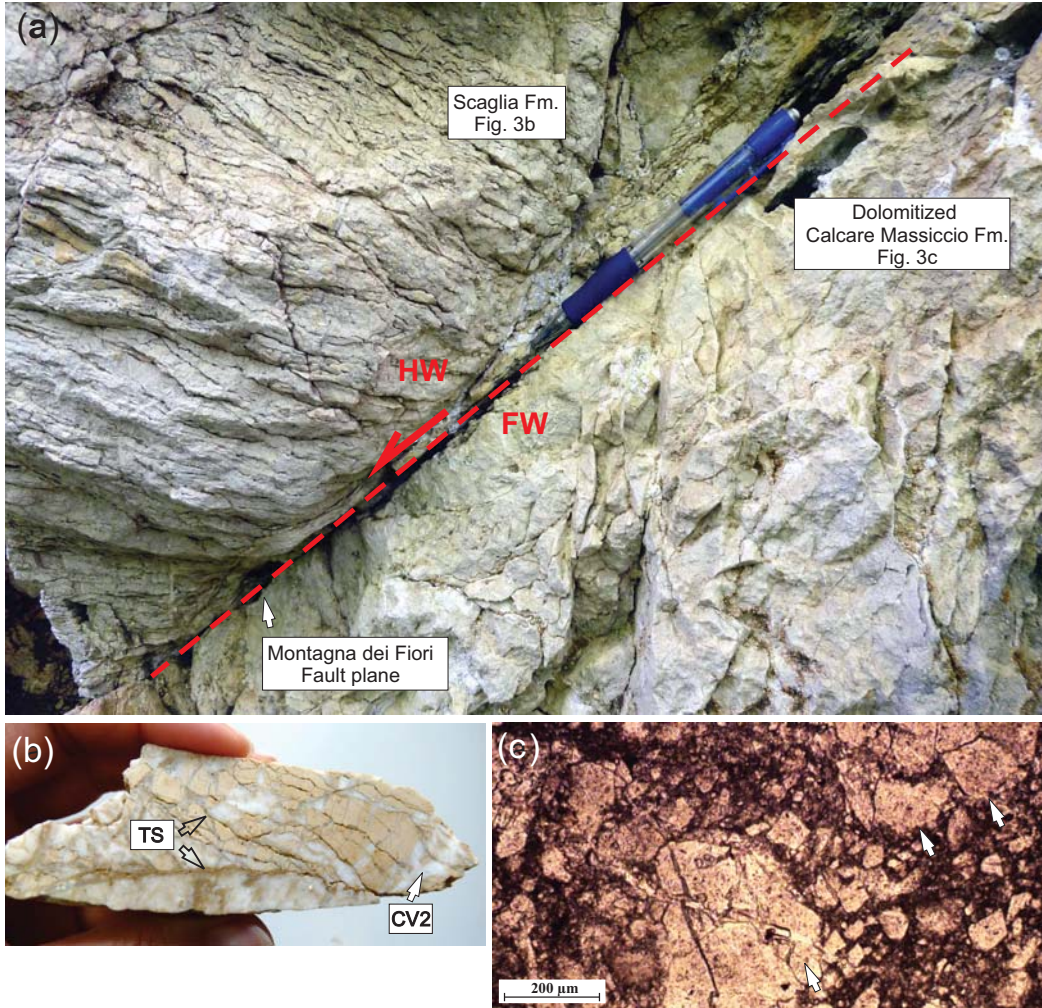


Fig. 3

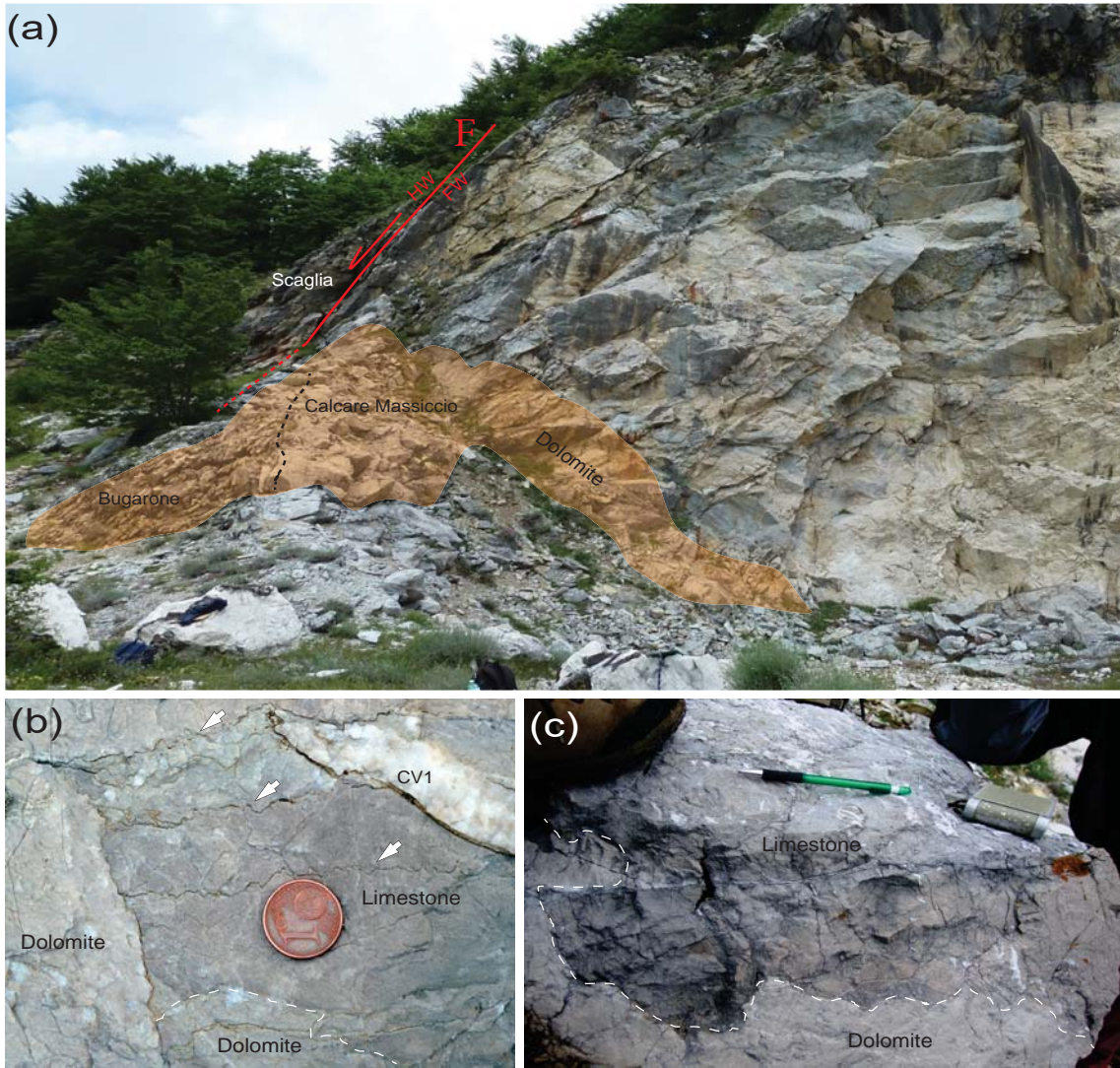


Fig. 4

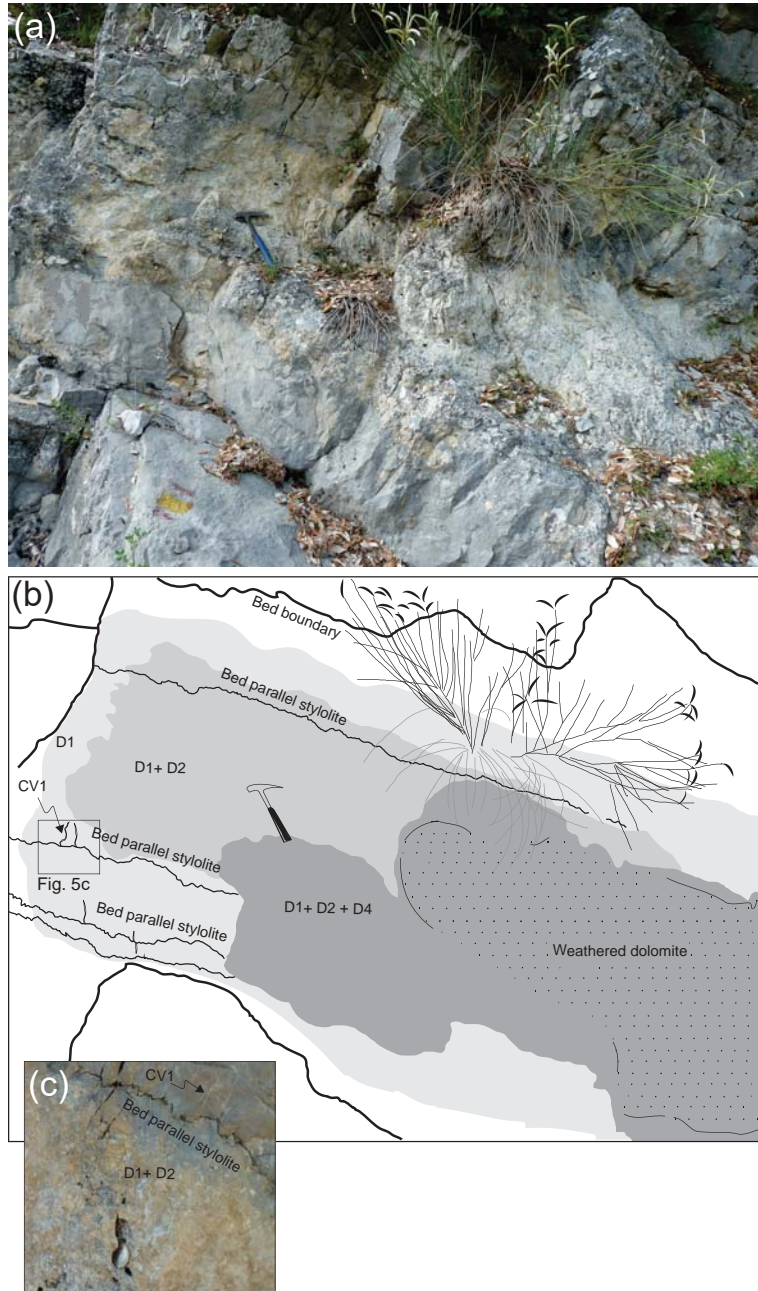


Fig. 5

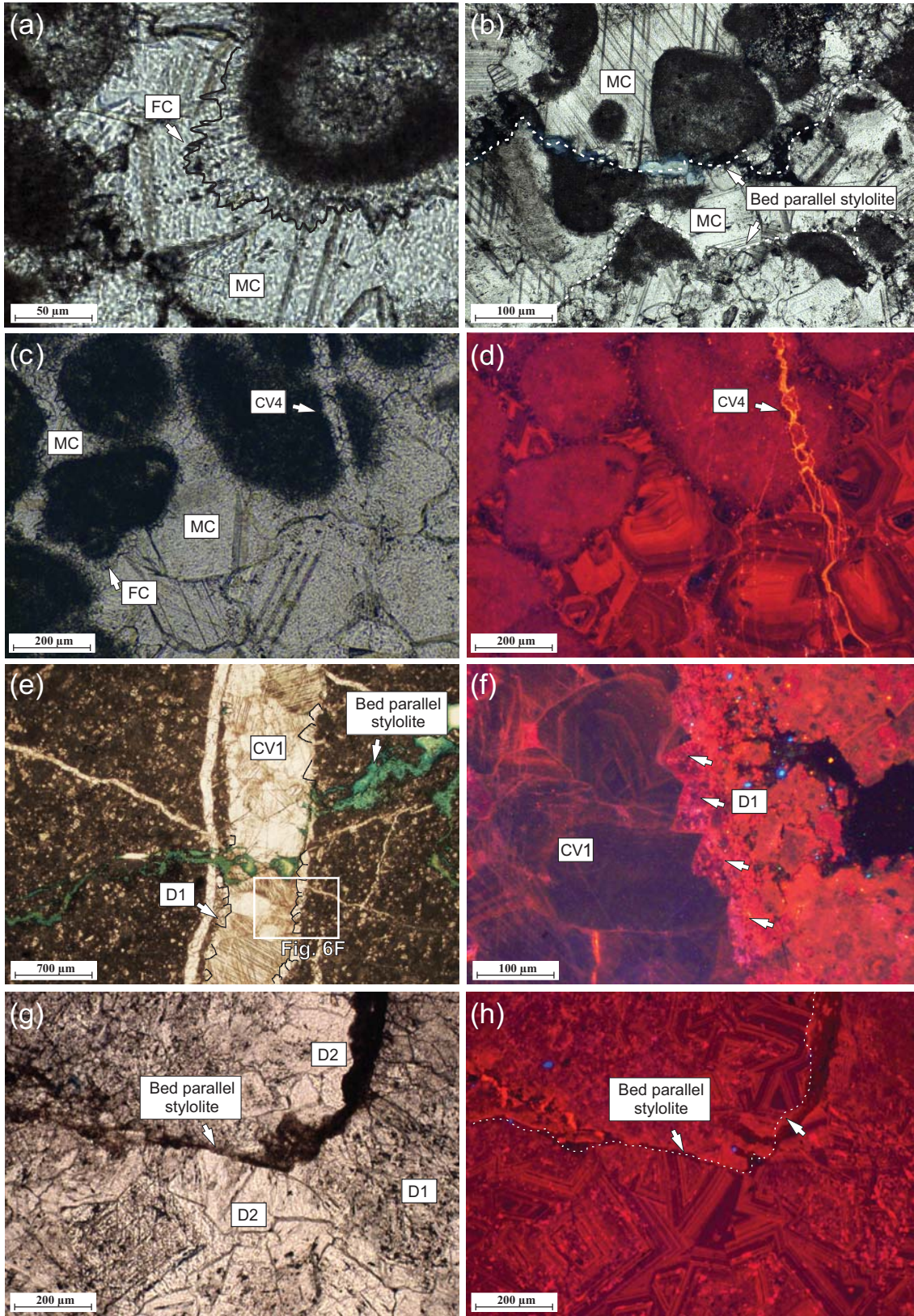


Fig. 6

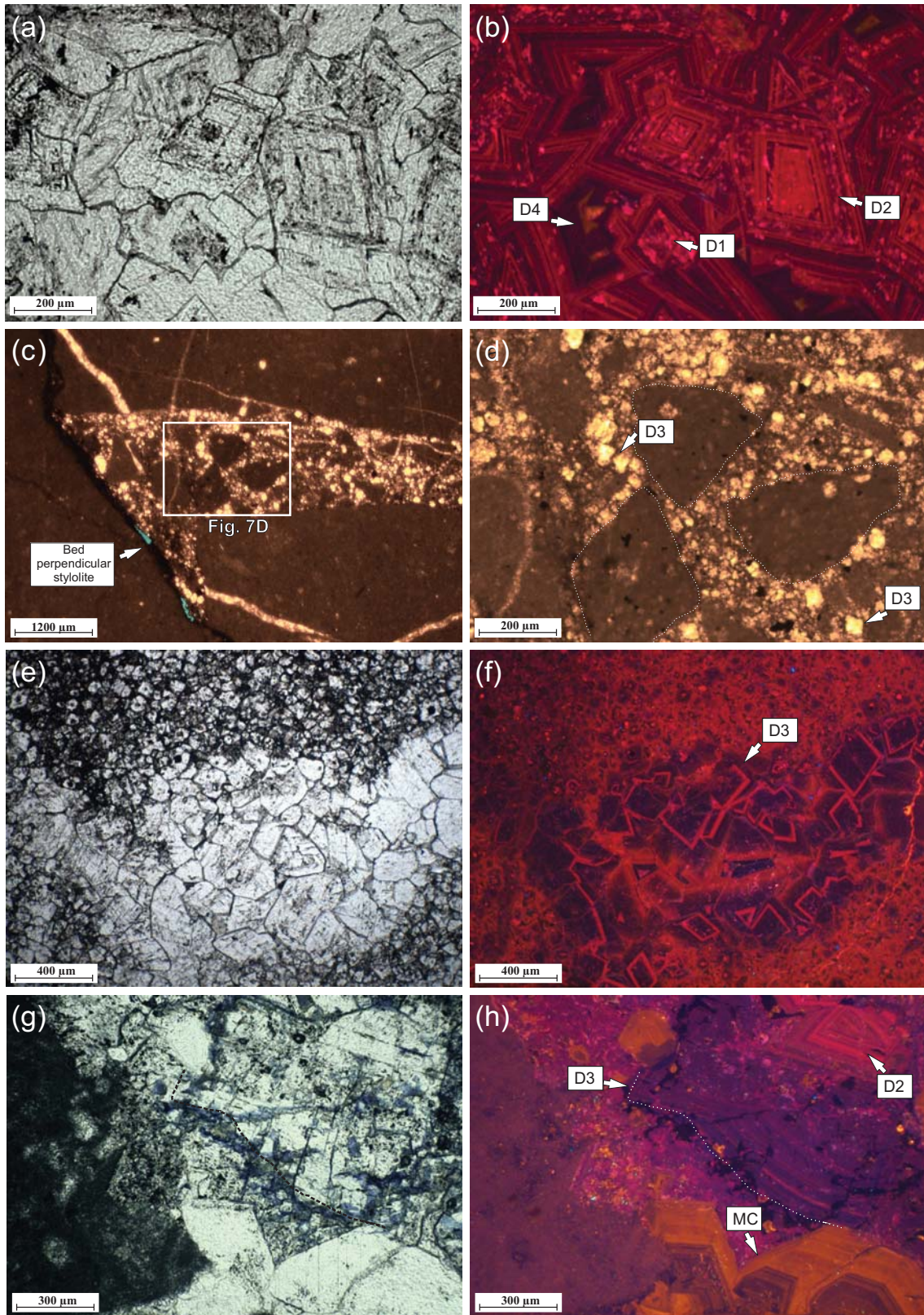


Fig. 7

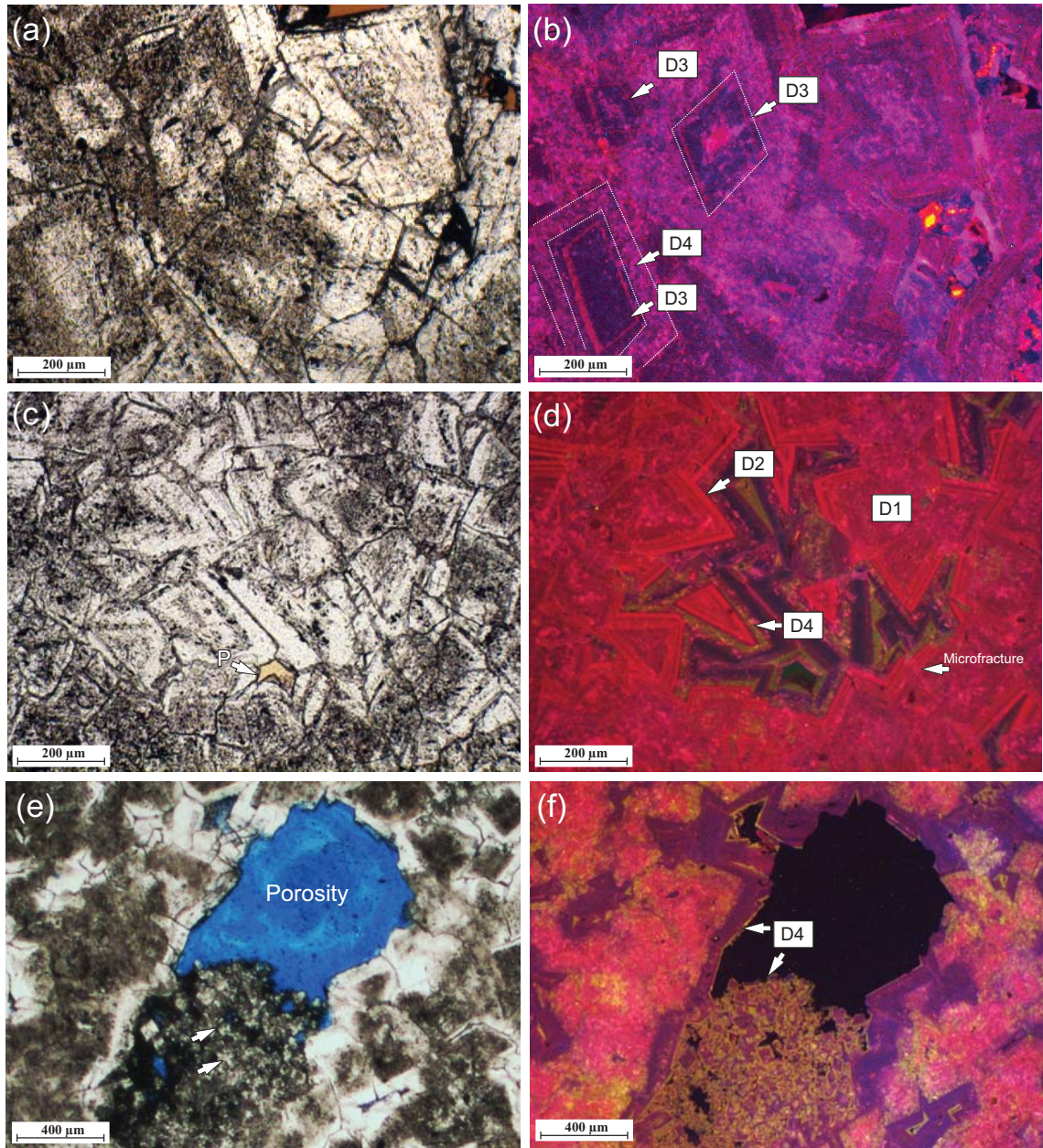


Fig. 8

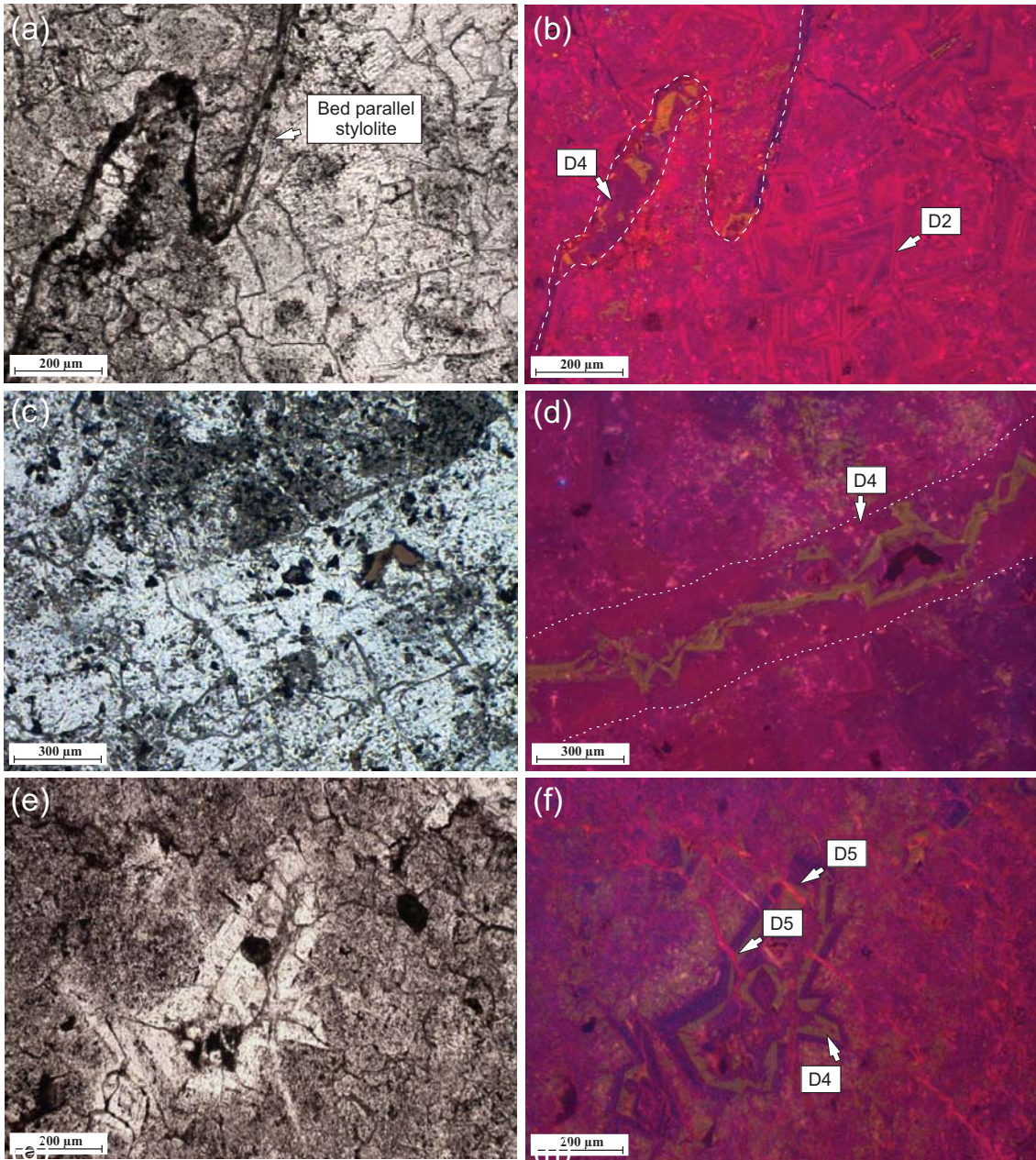


Fig. 9

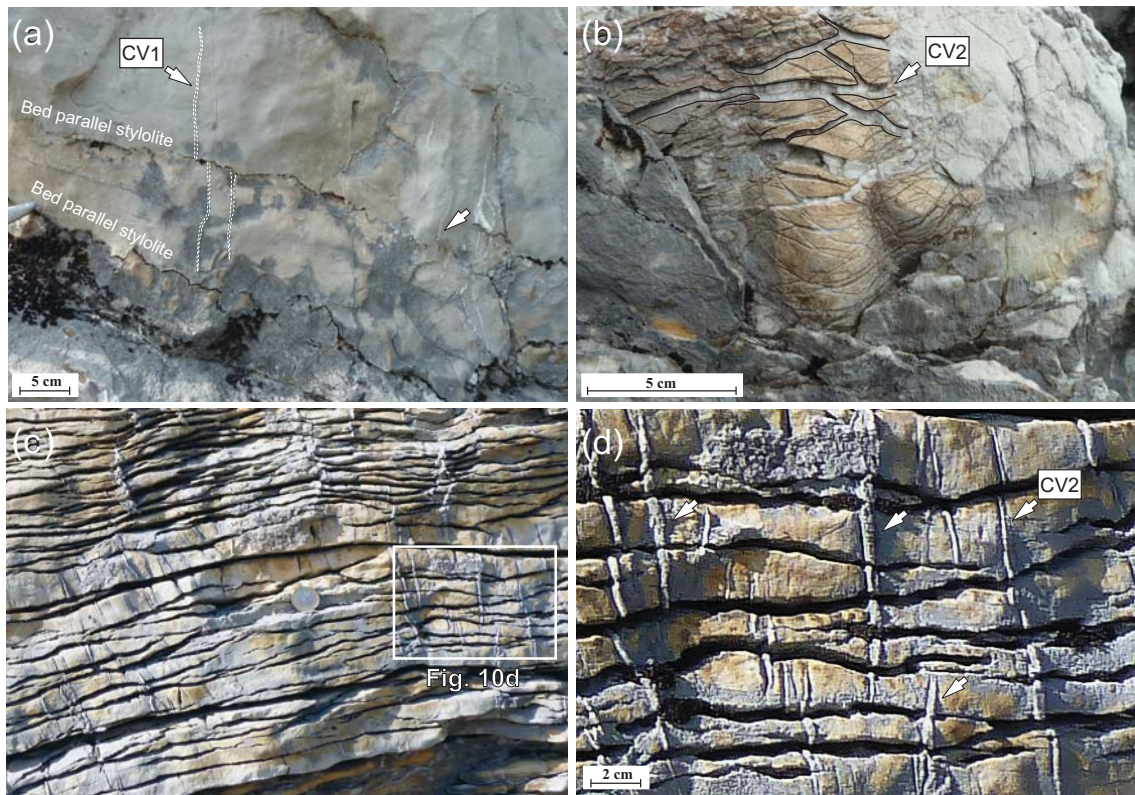


Fig. 10

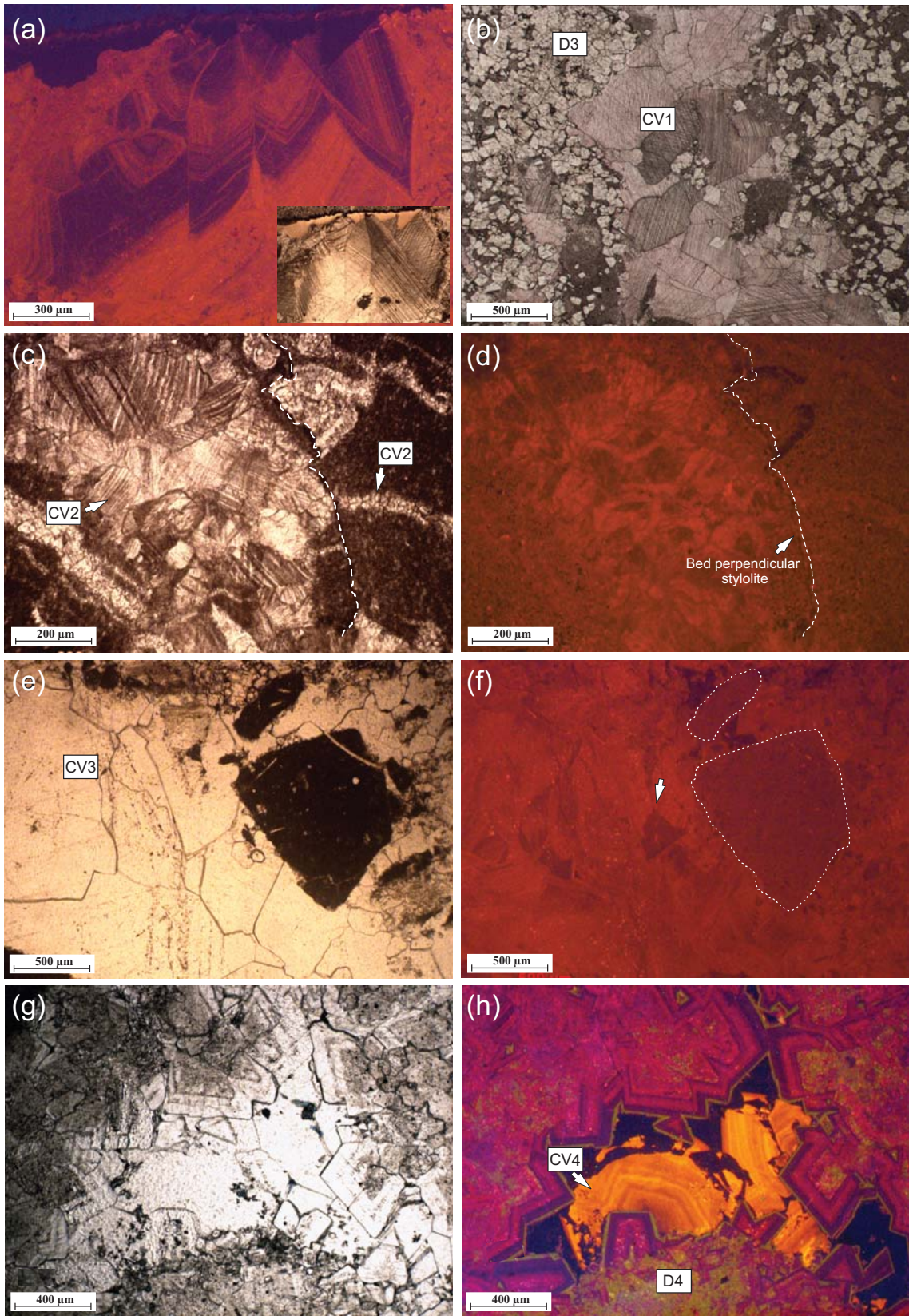


Fig. 11

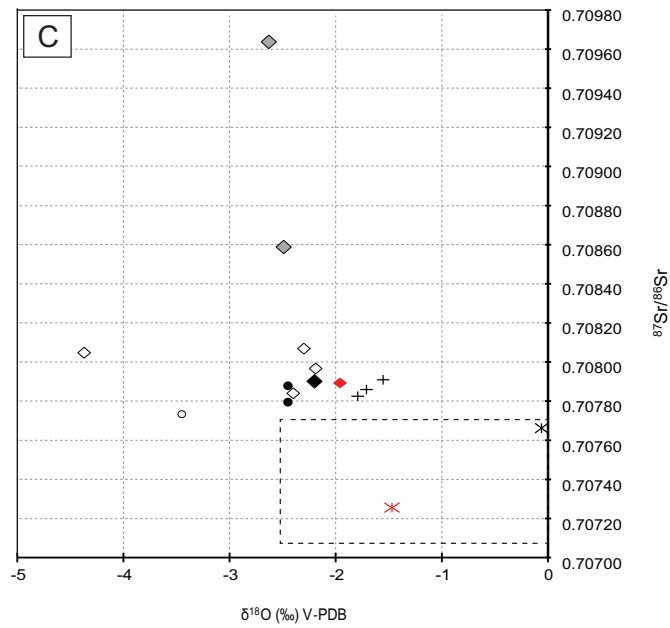
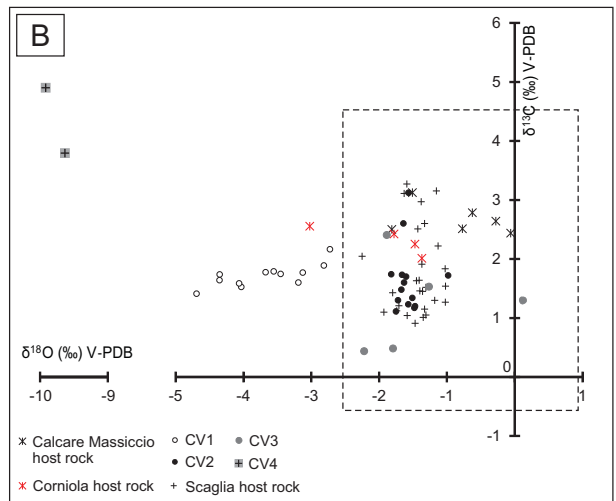
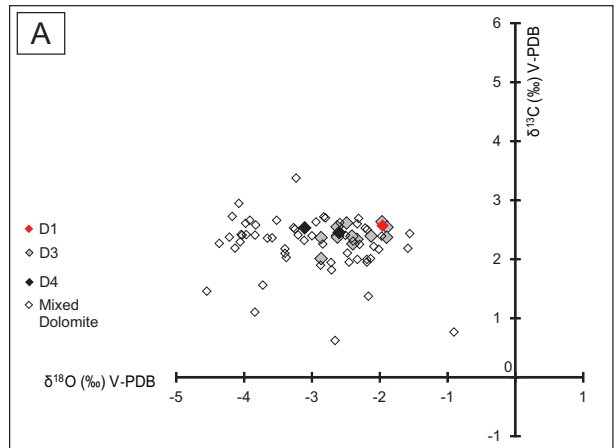


Fig. 12

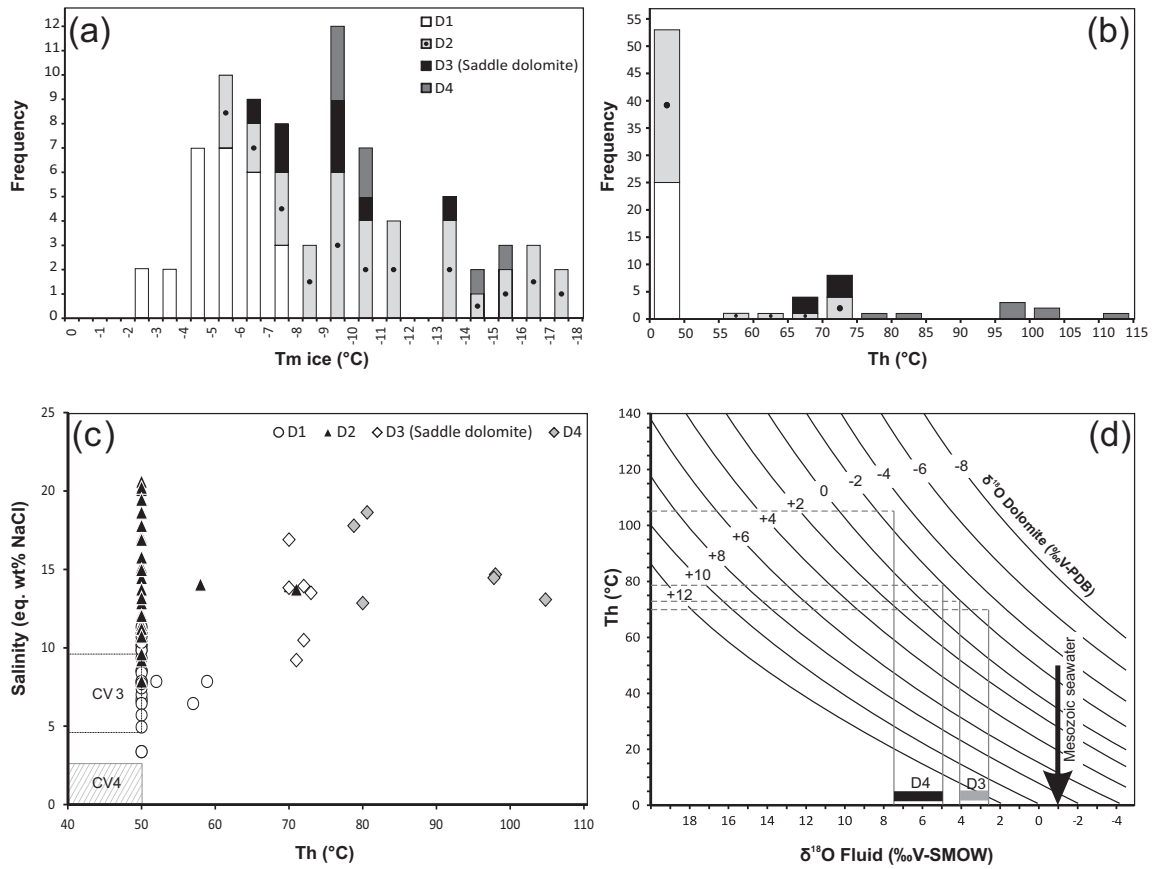


Fig. 13

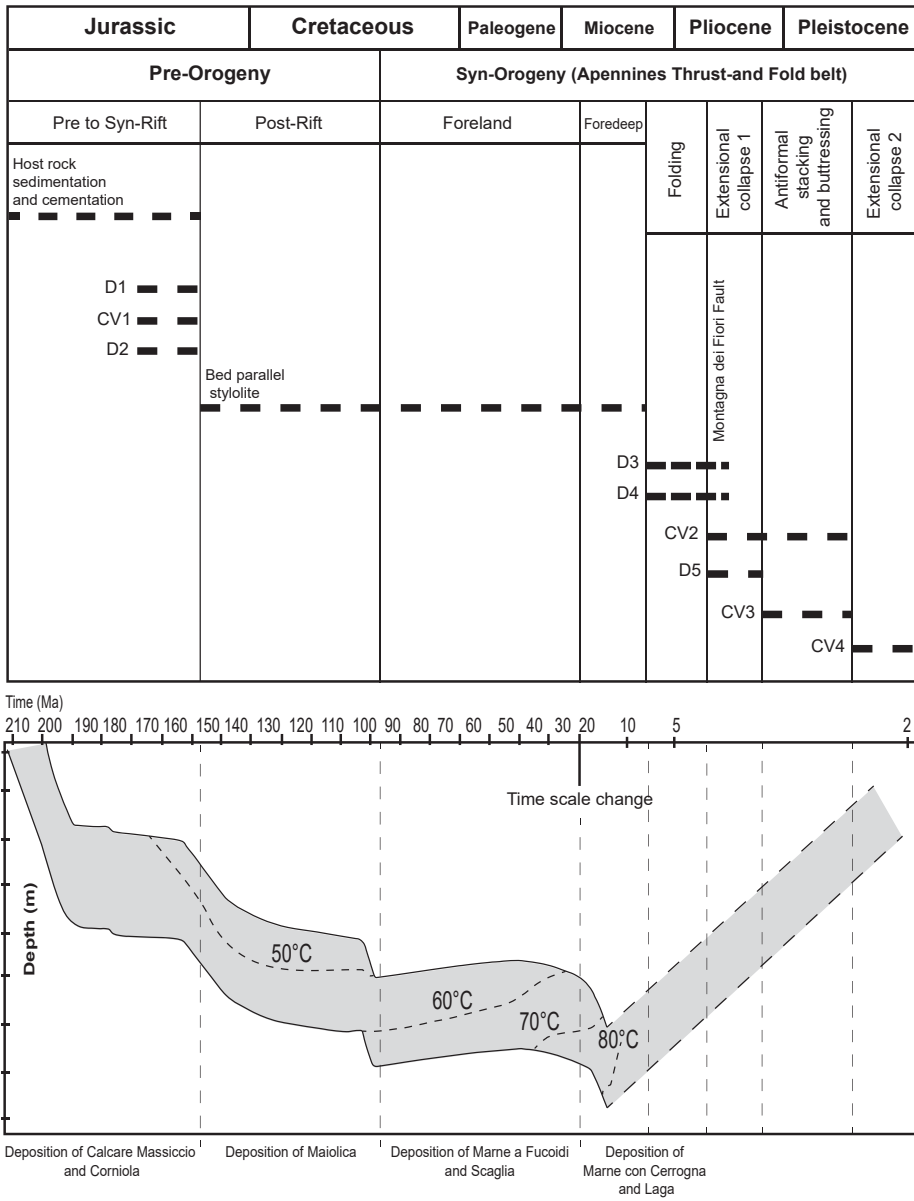


Fig. 14

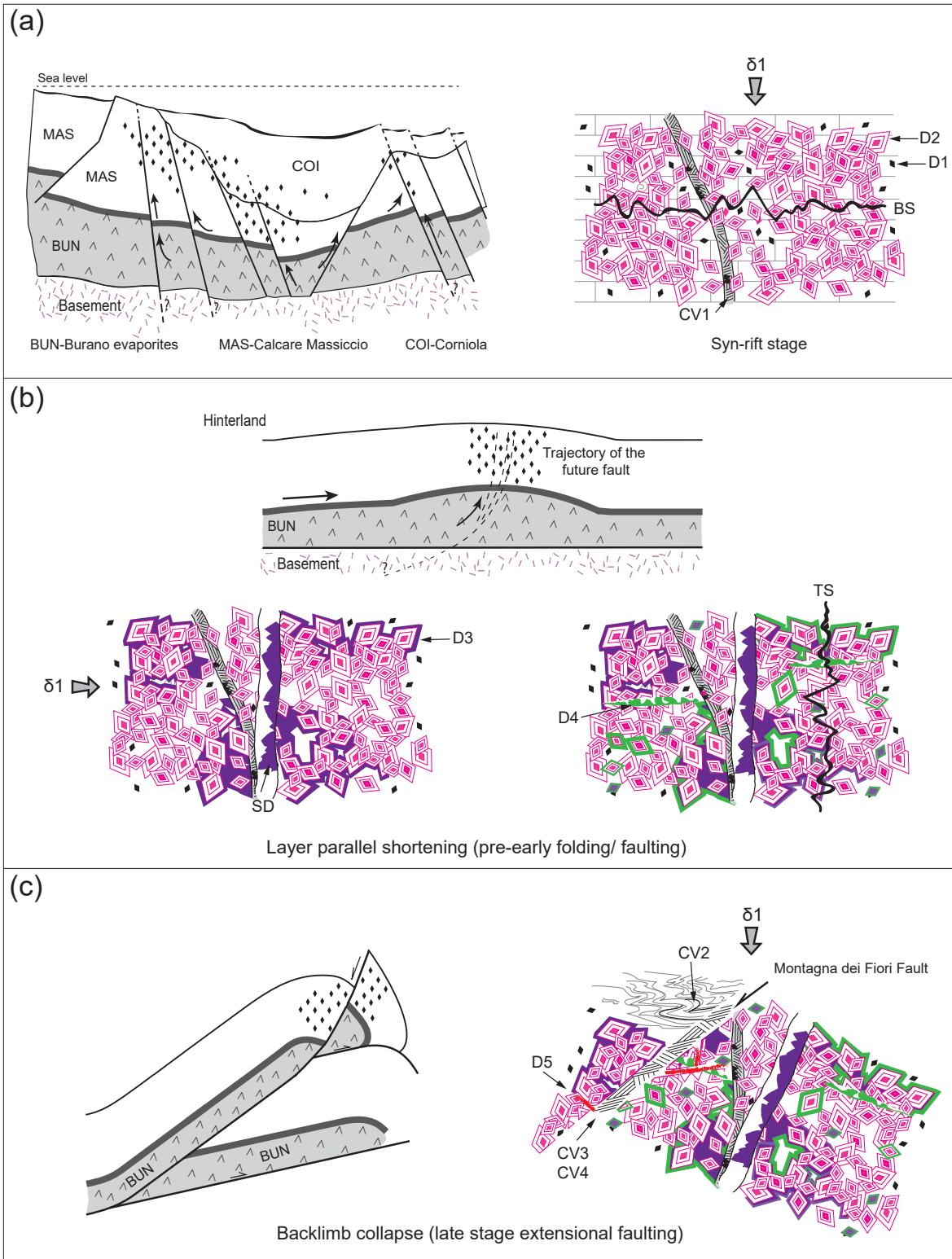


Fig. 15